Unveiling FKBP7 as an early endoplasmic reticulum sentinel in pancreatic stellate cell activation, collagen remodeling and tumor progression

Christophe Quemerais, Christine Jean, Alexia Brunel, Emilie Decaup, Guillaume Labrousse, Hippolyte Audureau, Jérôme Raffenne, Ismahane Belhabib, Jérôme Cros, Aurélie Perraud, et al.

Cancer Letters 614 (2025) 217538

Contents lists available at ScienceDirect

Cancer Letters

journal homepage: www.elsevier.com/locate/canlet

Original Articles

Unveiling FKBP7 as an early endoplasmic reticulum sentinel in pancreatic stellate cell activation, collagen remodeling and tumor progression

Christophe Quemerais [a], Christine Jean [a], Alexia Brunel [a], Emilie Decaup [a], Guillaume Labrousse [a], Hippolyte Audureau [a], Jérôme Raffenne [a], Ismahane Belhabib [a], Jérôme Cros [b], Aurélie Perraud [c], Nelson Dusetti [d], Remy Nicolle [e], Muriel Mathonnet [c], Stéphane Pyronnet [a], Yvan Martineau [a], Marjorie Fanjul [a], Corinne Bousquet [a,*]

[a] Cancer Research Center of Toulouse (CRCT), INSERM UMR-1037, CNRS UMR-5071, Team « Labellisée Ligue Contre le Cancer EL2021», University of Toulouse, France
[b] Department of Pathology, Beaujon-Bichat University Hospital - Paris Diderot University, Clichy, France
[c] EA 3842 Laboratory, Medicine and Pharmacy Faculties, University of Limoges, France
[d] Cancer Research Center of Marseille (CRCM), INSERM UMR-1068, CNRS UMR-7258, Marseille, France
[e] Center of Research on Inflammation (CRI), INSERM U1149, Paris, France

ARTICLE INFO

Keywords:
Pancreatic cancer
Pancreatic stellate cells
Cancer-associated fibroblasts
Endoplasmic reticulum
Collagen
Extracellular matrix
BiP

ABSTRACT

In pancreatic ductal adenocarcinoma (PDAC), fibroblast activation leads to excessive secretion of extracellular matrix (ECM) and soluble factors that regulate tumor progression, prompting investigation into endoplasmic reticulum (ER)-resident proteins that may support this activation. We identified FKBP7, a peptidyl-prolyl isomerase in the ER, as overexpressed in PDAC stroma compared to cancer cells, and in patients with favorable prognosis. Analysis of single-cell RNA sequencing databases revealed FKBP7 expression in pancreatic stellate cells (PSCs) and cancer-associated fibroblasts (CAFs). When analyzed by immunohistochemistry on PDAC patient tissues, FKBP7 emerged as an early activation marker in the preneoplastic stroma, preceding αSMA expression, and responding to FAK- and TGFβ-induced stiffening and pro-fibrotic programs in PSCs. Functional analyses revealed that FKBP7 knockdown in PSCs enhanced contractility, Rho/FAK signaling, and secretion of pro-inflammatory cytokines as well as remodeling of type I collagen, promoting an activated phenotype and accelerating tumor growth *in vivo*. Conversely, FKBP7 expression supported a tumor-restraining (i.e. encapsulating) ECM characterized by type IV collagen. Mechanistically, FKBP7 interacts with BiP, and blocking this interaction instead leads to increased PSC secretion of type I collagen. Thus, FKBP7 serves as a novel PSC marker and ER regulator in a complex with BiP of the secretion of specific collagen subtypes, highlighting its potential to mediate ECM normalization and constrain PDAC tumorigenesis.

1. Introduction

Pancreatic ductal adenocarcinoma (PDAC) is among the deadliest cancers, with a near 100 % mortality-to-incidence ratio and an increasing incidence that will likely make it the second leading cause of cancer-related deaths by 2030. Its high mortality stems from an often silent onset but rapid metastatic spread, limiting curative surgical options for most patients [1]. Despite aggressive poly-chemotherapy, patient survival gains remain limited, and immunotherapy has largely failed in PDAC [2–4].

Recent advances highlight the central role of the tumor microenvironment in PDAC aggressiveness and therapy resistance, suggesting that effective treatment will require multi-drug approaches targeting both cancer cells and their chemoprotective, immunosuppressive microenvironment [3,5]. PDAC is characterized by an extensive fibrotic stroma that can comprise up to 80 % of tumor volume and profoundly influences tumor biology. For instance, excessive extracellular matrix (ECM) deposition compresses blood vessels, making PDAC highly hypoxic and nutrient-poor, which drives metabolic reprogramming in both cancer and stromal cells that favors tumor progression [6–8]. The ECM in PDAC can also be spatially and structurally heterogeneous, forming thick collagen bundles that facilitate tumor cell

* Corresponding author. INSERM U1037, CRCT, 2 avenue Hubert Curien, CS53717, cedex1, 31037, Toulouse, France.
E-mail address: corinne.bousquet@inserm.fr (C. Bousquet).

https://doi.org/10.1016/j.canlet.2025.217538
Received 9 December 2024; Received in revised form 21 January 2025; Accepted 6 February 2025
Available online 7 February 2025

invasion and metastasis [9]. Cancer-associated fibroblasts (CAFs), which in PDAC largely derive from pancreatic stellate cell (PSC) activation, are the primary contributors to ECM deposition and stiffening [10]. PSCs are activated by tumor-derived factors like PDGF, SHH, and TGFβ early in tumorigenesis, initiating a pro-fibrogenic, pro-contractile reprogramming that promotes ECM remodeling and stiffening [8,11–14]. PSC-generated contractile force alters tumor biomechanical properties, causing compressive stress and pressure gradients on cancer cells. Tumor growth in confined spaces adds further stress. Latent TGFβ, stored in the ECM by binding proteins, is activated by mechanical forces [15], promoting epithelial to mesenchymal transition (EMT) and metastatic potential on cancer cells, and in a vicious cycle, further prompting CAFs to generate more force [16]. ECM remodeling provides structural tracks that cancer cells exploit for invasion [17,18].

Reprogrammed CAFs also secrete a variety of pro-tumorigenic factors, including growth factors and cytokines that support tumor growth, invasion, and chemoresistance [10]. This prolonged reprogramming is driven by epigenetic changes in CAFs [19]. CAF high protein production and secretion capacity in PDAC require high protein synthesis, facilitated by increased mTOR-dependent mRNA translation [20].

Targeting this CAF reprogramming—particularly its protein secretion machinery—could reveal potential therapeutic vulnerabilities. Targeting the stroma is now seen as essential to improve PDAC treatment outcomes [21]. However, genetic mouse models that depleted activated fibroblasts expressing the marker αSMA at either early or late stages of PDAC progression, or that deleted Shh in cancer cells resulting in abrogation of stromal formation, showed accelerated disease and increased aggressiveness [22,23], and a Shh antagonist failed in the clinic [24]. In addition, therapeutic approaches using ECM-modifying enzymes showed encouraging results in preclinical models, but also failed in clinical trials [25,26]. Nevertheless, antifibrotic drugs appear to be effective in normalizing the stroma and blocking tumor progression, at least in preclinical models [27,28]. These data underscored the question of whether the stroma acts as a friend or a foe [29] and highlighted the need for a deeper understanding of PDAC stroma biology, including its heterogeneity, which may explain these controversies [8,30].

We reasoned that increased protein secretion in CAFs implies adaptive mechanisms in the endoplasmic reticulum (ER), since most membrane-bound and secreted proteins are synthesized on ER-associated ribosomes. These proteins enter the ER in an unfolded state, where chaperones assist in protein folding and stabilization. The ER maintains protein homeostasis through the unfolded protein response (UPR), adjusting folding capacity based on cellular needs. ER stress occurs when folding demands exceed capacity, triggering sensors that activate the UPR to restore balance [31,32].

In this study, we explored ER adaptations supporting the increased protein synthesis in PSCs as they reprogram into CAFs. We identified FKBP7, an ER-resident peptidyl prolyl isomerase (PPI), as a key protein overexpressed in the stroma compared to epithelial tissues in both pancreatitis and PDAC samples from human and murine models. FKBP7 has been described as a regulator of BiP, a major heat shock protein (Hsp) 70 chaperone in the ER, where it negatively affects BiP ATPase activity and contributes to protein synthesis regulation [33,34]. Here, we investigated how FKBP7 expression is regulated and its function in PDAC.

Our findings show that FKBP7 expression in PSCs increases in response to TGFβ and stiffness signals, both early events in pancreatic tumorigenesis. FKBP7 acts as a negative feedback regulator that limits PSCs from fully adopting the contractile and pro-inflammatory traits typical of the CAF pro-tumor phenotype. By restraining these characteristics, FKBP7 may counteract some of the pro-tumorigenic functions attributed to CAFs, highlighting its potential as a therapeutic target in PDAC stroma management. Mechanistically, we provide evidence that distinct collagen subtypes are produced by PSCs dependently on the expression of FKBP7 and interaction with BiP. This novel understanding of FKBP7 role in PSC activation provides insights into how ER chaperones might influence stromal reprogramming and CAF functions in PDAC, offering new avenues for stromal-targeted interventions in this aggressive cancer.

2. Materials and methods

2.1. Cell isolation, genetic modifications, culture and treatments

Human CAFs: they were isolated from patient pancreatic tumor tissues using the outgrowth method described by Bachem et al. [35]. Briefly, cells were isolated using explant techniques from histologically fibrotic areas of surgically resected PDAC. Human pancreatic tumor tissues were obtained from the Pathology Department of Limoges Hospital, France, from patients undergoing pancreatic resections for pancreatic adenocarcinoma (Convention CRB/MAD-CC-2013-002). Small tissue blocks were cut (0.5–1 mm^3) using razor blade and seeded in 10-cm^2 culture wells in Dulbecco's modified Eagle's medium F12 (DMEM/F12, Sigma-Aldrich) containing L-Glutamine (LGln) and supplemented with 10 % fetal calf serum (FCS) (Eurobio), penicillin and streptomycin (P/S). Tissue blocks were cultured at 37 °C in a 5 % CO2-air humidified atmosphere. Eighteen hours after seeding, culture medium was changed. CAFs grew out from the tissue blocks 1–3 days later. CAF primary cultures were immortalized *via* retrovirus-mediated expression of human telomerase reverse transcriptase (hTERT). An authorization for collecting and conserving this collection was given by the Comité de protection des personnes Sud-Ouest et Outre-Mer II (Déclaration de conservation et préparation de collections DC-2016-2654). This study was approved by the ethic committee of the Institution.

Human PSCs: PSCs were isolated from suspension of human dissociated healthy pancreas adjacent to patient tumor, according to a slightly modified protocol [36]. Briefly, pancreas suspension was incubated during 7min with digestion buffer (0.05 % collagenase P, 0.1 % DNAse, 0.02 % pronase) in a freshly prepared Gey's Balanced Salt Solution (GBSS) (Sigma-Aldrich). The digested sample was filtrated through 100 μm nylon mesh, centrifuged at 1800 rpm for 8min and washed with 0.3 % BSA in GBSS. After centrifugation, the pellet was resuspended in 0.3 % BSA GBSS and mixed in a 35.6 % Nycodenz solution (Alere Technologies). The Nycodenz gradient was prepared by layering 22 ml of cell suspension in Nycodenz underneath 9 ml of 0.3 % BSA GBSS in a 50 ml centrifuge tube. After a centrifugation at 2600 rpm for 20min (with an off brake), PSCs present at the interface were harvested, washed with 40 ml of PBS plus P/S, centrifuged 8min 1800 rpm, resuspended in DMEM/F12 10 % FCS plus P/S into 6-well poly-L-lysine plate. Medium was changed after 45min, and primary PSCs were expanded, frizzed and/or been immortalized *via* retrovirus-mediated expression of hTERT. PSCs were grown in adherent culture, as for CAFs.

Mouse embryonic fibroblasts (MEFs): MEFs were isolated from E8.5 embryo explant culture, and were expanded and maintained on dishes pre-coated with 0.1 % gelatin (Sigma-Aldrich) in DMEM/F12 10 % FCS plus P/S and LGln. After expansion and limited passage, primary MEFs were immortalized *via* retrovirus-mediated expression of human telomerase reverse transcriptase (hTERT) followed by puromycin selection, or spontaneously immortalized.

Stable cell lines knocked-down for FKBP7 or overexpressing wild-type or mutant FKBP7: To decrease FKBP7 expression in a stable-dependent manner, four distinct shRNAs targeting FKBP7 (sh399, sh000, sh001 and sh002) were engineered and packaged using the lentivirus delivery system from the following FKBP7 shRNA plasmids (sh399 TRCN00005399, and sh000 TRCN000054000) and from the shRNA control (CTR) pLKO.1-puro non-mammalian plasmid (SHC002) (Sigma-Aldrich). PSCs and CAFs were transduced with lentivirus shFKBP7 or shCTR, using protamine sulfate at 10 μg/mL in Opti-MEM I Reduced Serum Medium. After 12 h of transduction, the transduction medium was replaced by puromycin-selecting medium at 1 μg/mL. PSCs

and CAFs transduced with shFKBP7 #399 or #000 only resulted in at least 60 % decrease of FKBP7 expression compared to shCTR by Western blot analysis, and were kept for further analyses. To overexpress FKBP7 in cells, the lentivector ploc FKBP7 (OHS5897, Discovery Horizon), or control vector ploc CTR lacking the FKBP7 sequence, was transduced in PSCs and CAFs as described above except that a blasticidin-selecting medium was used at 3 μg/mL. FKBP7 mutants were engineered using different G-blocks (Integrated DNA Technologies), to delete the FKBP7 PPI (peptidyl prolyl isomerase) domain (deletion of nucleotides 159–378, GenBank: BT007122.1), or the FKBP7 C-terminal domain (deletion of nucleotides 435–654, GenBank: BT007122.1); (G-block PPI domain: TAA ACT TAA GCT TGG TAC CGA GCT CGG ATC CAC TAG TCC AGT GTG GTG GAA TTC TGC AGA TAT CAC AAG TTT GTA CAA AAA AGC AGG CTC CAC CAT GCC AAA AAC CAT GCA TTT CTT ATT CAG ATT CAT TGT TTT CTT TTA TCT GTG GGG CCT TTT TAC TGC TCA GAG ACA AAA GAA AGA GGA GAG CAC CGA AGA AGT GAA AAT AGA AGT TTT GCA TCG TCC AGA AAA CTG CTC TAA GAC AAG CAA GAA GGG AGA CCT ACT AAA TGC CCA TTA TGA CGG CTA CCT GGC TAA AGA CGG CTC GAA ATT CTA CTG CAG CCG GAC ACA AAA TGA AGG CCA CCC CAA ATG GTT TGT TCT TGG TGT TGG GCA AGT CAT AAA AGG CCT AGA CAT TGC TAT GAC AGA TAT GTG CCC TGG AGA AAA GCG AAA AGT AGT TAT ACC CCC TTC ATT TGC ATA CGG AAA GGA AGG CTA TGC AGA AGG CAA GAT TCC ACC GGA TGC TAC ATT GAT TTT TGA GAT TGA ACT TTA TGC TGT GAC CTA CCC ATA CGA TGT TCC AGA TTA CGC TCA CGA TGA ACT ATG AAT CCA CCC AGC TTT CTT GTA CAA AGT GGT TGC TAG CTA ATG AAC CGG GCG CGC CCC GCC CC); (G-block C-terminal domain: TAA ACT TAA GCT TGG TAC CGA GCT CGG ATC CAC TAG TCC AGT GTG GTG GAA TTC TGC AGA TAT CAC AAG TTT GTA CAA AAA AGC AGG CTC CAC CAT GCC AAA AAC CAT GCA TTT CTT ATT CAG ATT CAT TGT TTT CTT TTA TCT GTG GGG CCT TTT TAC TGC TCA GAG ACA AAA GAA AGA GGA GAG CAC CGA AGA AGT GAA AAT AGA AGT TTT GCA TCG TCC AGA AAA CTG CTC TAA GAC AAG CAA GAA GAC CAA AGG ACC ACG GAG CAT TGA GAC ATT TAA ACA AAT AGA CAT GGA CAA TGA CAG GCA GCT CTC TAA AGC CGA GAT AAA CCT CTA CTT GCA AAG GGA ATT TGA AAA AGA TGA GAA GCC ACG TGA CAA GTC ATA TCA GGA TGC AGT TTT AGA AGA TAT TTT TAA GAA GAA TGA CCA TGA TGG TGA TGG CTT CAT TTC TCC CAA GGA ATA CAA TGT ATA CCA ATA CCC ATA CGA TGT TCC AGA TTA CGC TCA CGA TGA ACT ATG AAT CCA CCC AGC TTT CTT GTA CAA AGT GGT TGC TAG CTA ATG AAC CGG GCG CGC CCC GCC CC). G-block recombination with the ploc CTR plasmid generated two plasmids containing either a FKBP7 mutant lacking the PPI domain (ΔPPI), or a FKBP7 mutant lacking the C-terminal domain (ΔC-ter), from which lentivirus were produced and transduced in PSCs, as described above.

Cell treatments: FAK inhibitor (PF-562271, Selleckchem, #S2890) was added at 1 μM on cells pre-starved in DMEM/F12 0.5 % FCS overnight. Thapsigargin (3 μM), tunicamycin (8 μg/mL), Brefeldin A (0.5 μg/mL), or TGFβ (8 ng/mL) were added on adherent cells cultivated in complete medium (10 % FCS) for a timing described in the figure legends.

2.2. Western blot

Cell lysis was performed in lysis buffer (20 mmol/L Tris, pH 7.5, 150 mmol/L NaCl, 1 mmol/L EDTA, 1 % NP40, 1 mmol/L sodium orthovanadate, 1 mmol/L NaF, and a cocktail of protease inhibitors (Roche)).

The protein extract concentration was measured using the Protein Assay reagent (Bio-Rad). Equal amounts of proteins were resolved by sodium dodecyl sulfate–polyacrylamide gel electrophoresis and electroblotted onto nitrocellulose membranes. Membranes were blocked (5 % powdered milk in Tris-buffered saline with 0.1 % Tween 20) followed by incubation with primary antibodies (see Table S1). Membranes were then incubated with horseradish-peroxidase–coupled secondary antibody and treated with Pierce ECL Western Blotting Substrate before detection with the PXi imaging system (Syngene).

2.3. SUnSET assay

SUnSET assay, a nonradioactive equivalent of ^{35}S-Met assay based on puromycin incorporation into nascent polypeptides [37], was used to monitor the rate of protein synthesis using an anti-puromycin antibody. Briefly, 10 min prior cell harvesting, puromycin was added to culture medium at 1 μg/mL. CAFs, PSCs or tumor cells extracts were then processed for Western blotting using anti-puromycin antibody (see Table S1).

2.4. Co-immunoprecipitation

Cell lysis was performed in lysis buffer (20 mmol/L Tris, pH 7.5, 150 mmol/L NaCl, 1 mmol/L EDTA, 0.5 % NP40, 1 mmol/L sodium orthovanadate, 1 mmol/L NaF, and a cocktail of protease inhibitors; Roche). Four-hundred μg of cellular extracts were incubated overnight with Protein G sepharose beads (Ge Healthcare # 170618-01) and anti-FKBP7 or anti-HA antibody (see Table S1) or irrelevant antibody as immunoprecipitation control (anti-FLAG antibody, CST 14793S). After four bead-washes with lysis buffer, immunoprecipitated proteins were analyzed by SDS-PAGE. The inputs represent 10 % of total lysates used for immunoprecipitation.

2.5. Subcellular fractionation

To isolate cytosolic fraction, cell pellets were resuspended with cytosolic extraction buffer containing (Nacl 150 mM, Hepes 50 mM pH 7.4, EGTA 0.1 mM, DTT 1 mM, a cocktail of protease inhibitors and digitonine at 100 μg/mL). After 10 min on ice, cell suspensions were centrifugated at 2000 rpm during 10 min and cytosolic fractions which correspond to supernatant were collected. Then, after two washes with the cytosolic extraction buffer, cell pellets were resuspended with membrane extraction buffer containing (Nacl 150 mM, Hepes 50 mM pH 7.4, EGTA 0.1 mM, DTT 1 mM, a cocktail of protease inhibitors and NP40 0.5 %). After 30 min on ice, cell lysates were centrifugated at 7000 rpm during 5 min. Cell supernatants corresponding to the membrane fractions (plasma membrane + organelles) were collected. Both cytosolic and membrane fractions were analyzed by SDS-PAGE.

2.6. Immunofluorescence

Human CAFs or PSCs cultured on glass coverslips were fixed (10 min, 10 % formalin) and permeabilized (10 min, 0.05 % Triton X-100). After blocking with 3 % BSA for 1 h, they were incubated with primary antibodies (see Table S1) in PBS-3% BSA overnight at 4 °C. Cells were PBS washed and incubated with the appropriate Alexa Fluor secondary antibodies, plus TRITC-phalloidin (1:1000, Sigma) for 1 h at room temperature (RT). After PBS washes, nuclei were stained with DAPI (1:1000, Sigma-Aldrich) for 10 min. After PBS washes, coverslips were mounted in Fluorescent mounting medium (Dako). Images were acquired using a confocal Zeiss LSM 780 microscope. For quantification, fields were chosen arbitrarily and the mean fluorescence intensity (MFI) was quantified on regions of interest (ROI) using Zen 2.3 lite software (Zeiss). ROIs were defined by random freehand selection of cells based on phalloidin staining, after background subtraction. When samples were decellularized, cell cultures were used at confluence to ensure equivalent cell density, and then decellularized and stained for type I or IV collagens, which was quantified on the whole samples.

For immunofluorescence staining of deposited collagens (decellularized samples), confluent PSCs cultured on glass coverslips were treated with alkaline detergent extraction buffer (0.5 % Triton X-100, 20 mM NH_4OH in PBS). After 2 min, coverslips were washed with PBS and DNase treated (10 μg/mL) for 30 min at 37 °C, then washed with PBS. Immunofluorescence staining was then performed to detect type I or type IV collagens, as described above. Corresponding MFI were quantified on fields chosen arbitrarily using Zen 2.3 lite software (Zeiss).

Collagen fiber alignment was determined using the Directionality plugin in ImageJ. This plugin is used to infer the preferred orientation of structures present in the input image. It computes a histogram indicating the amount of structures in a given direction. Images with completely isotropic content are expected to yield a flat histogram, while images with a preferred orientation are expected to yield a histogram with a peak at that orientation. This method is based on Fourier spectral analysis. For a square image, structures with a preferred orientation produce a periodic pattern at +90° orientation in the Fourier transform of the image, compared to the direction of the objects in the input image. On top of the histogram, the plugin generates statistics on the highest peak found, which is fitted by a Gaussian function, taking into account the periodic nature of the histogram. For each image, the plugin cuts it into square pieces, and computes their Fourier power spectra, thus ensuring multiple field analysis per sample. The "dispersion" parameter indicates the standard deviation of the Gaussian.

2.7. Histological analysis: colorations, immunohistochemistry and immunohistofluorescence

Paraffin-embedded tissue sections were incubated 30 min at 60 °C before being deparaffinized and rehydrated. For hematoxylin-eosin (H&E) staining, slides were then incubated 3 min in hematoxylin, washed 5 min in water, incubated 3 min in eosin and dehydrated in 100 % ethanol before being cleared in xylene for 5 min and mounted using Eukitt. For picrosirius red staining, deparaffinized and rehydrated sections were incubated with picrosirius red solution (Abcam) for 1h, rinsed quickly in 0.5 % acetic acid, dehydrated, cleared and mounted in Eukitt. Sections were analyzed using Cell Observer widefield microscope (Zeiss) with polarizer D, 90° rotatable for Axio Observer (Zeiss). Areas of yellow-orange birefringent fibers corresponding to thick fibers and green birefringent fibers corresponding to thin fibers were quantified using ImageJ software.

For immunohistochemical (IHC) and immunohistofluorescence (IHF) stainings, after rehydration, sections were processed for antigen retrieval (10 mM Tris-EDTA pH9 and autoclaved at 120 °C for 12 min) and quenched or not (IHF) for peroxidase activity (10 min with 0.3 % hydrogen peroxide at RT) before being washed 5 min in PBS. After treatment with blocking buffer (45 min, RT), sections were incubated with primary antibodies (see Table S1) overnight at 4 °C. Sections were PBS-washed and incubated (1h, RT) with ImmPRESS secondary antibodies (IHC) or appropriate Alexa Fluor-conjugated secondary antibodies (IHF). For IHC, after PBS washes, antibody binding was visualized with AEC (3-Amino-9-ethylcarbazole) chromogen substrate and counterstained with hematoxylin (2 min). Slides were washed with water,mounted using Glycergel and imaged with a Panasonic 250 scanner (Imag'IN core, Institut Universitaire du Cancer Toulouse, France). For IHF after PBS washes, nuclei were stained with DAPI (1:1000, 10 min, RT) and slides were mounted with fluorescent mounting medium. Images were acquired using a confocal Zeiss LSM 780 microscope.

2.8. Electron microscopy

For scanning electron microscopy (SEM) analysis, cells were grown on glass coverslips, fixed in glutaraldehyde 2.5 % in cacocylate buffer (0.1M, pH 7.4) (Electron Microscopy Sciences) for 1h and then washed with distilled water. After dehydratation, samples were mounted on microscope stubs followed by platinum sputtering. Specimens were examined on a FEI Quanta 250 FEG scanning electron microscope at 10 kV accelerating voltage.

2.9. High content screen (HCS)

PSCs overexpressing FKBP7 or not were plated (5000 cells/well) in 96-well plate with optically clear bottom (PerkinElmer). After 48h, cells were fixed for 30 min at RT with paraformaldehyde 4 %, 3-times washed with PBS and permeabilized with PBS/0.2 % Triton-X-100 for 20 min at RT. After 3 PBS-washes, non-specific antibody binding was reduced by a blocking step with 3 % BSA in PBS for 1 h at RT. Antibodies targeting FKBP7 and αSMA (see Table S1) were added in 3 % BSA in PBS, overnight at 4 °C. After 3 PBS-washes, cells were incubated with the secondary antibodies (Alexa Fluor-546 for FKBP7, and Alexa Fluor-647 for αSMA) for 1h. Antibodies were removed by 3 PBS-washes and nuclei were stained with DAPI (1:1000, 10 min). After an additional PBS-wash, 96-well plates were sealed and images were acquired with an Operetta CLS High Content Imaging system from PerkinElmer at 20x air objective and processed using Harmony software (version 4.9). Nuclei, αSMA and FKBP7 images were acquired in the DAPI (blue), Alexa 546 (Red) and Alexa 647 (Far red) channels, respectively. After data acquisition, subsequent analyses were performed with Columbus software (version 2.8.2). Image analysis was performed using a custom made image analysis protocol [38], with quantification of total number of cells, of number of activated cells based on per cell αSMA MFI, and of per cell αSMA fiber length.

2.10. MTT assay

Cells were seeded in 96-well plates (5000 cells/well for PSCs or CAFs, and 7500 cells/well for tumor cells) and treated if needed. At time described in the figure, MTT, (4,5-dimethylthiazol-2-yl)-2,5-diphenyl tetrazolium (Life Technologies) was added to each well at 0.5 mg/mL for 2 h. Hundred µL of dimethylsulfoxide were added for 1 h to each well. Viability was estimated by measuring absorbance at 570 nm on MRX plate reader (Dynex Technologies).

2.11. Collagen gel contraction assay

Collagen lattices were prepared using rat tail type I collagen (Corning, #354249) according to the manufacturer's instructions. FKBP7 knock-down or overexpressing PSCs and CAFs were trypsinized, counted for dilution at 2×10^5 cells/mL, suspended in collagen (1 mg/mL of collagen final concentration) and plated into 24-well plates (500 µL/well). Collagen lattices were kept for 2 h at RT for polymerization. To initiate collagen gel contraction, polymerized gels were gently released from the underlying culture dish and DMEM/F12 10 % FCS medium was immediately added. The degree of collagen gel contraction was analyzed during 4 days. Gel surface was measured using ImageJ software. Gel contraction = 100*(well surface - gel surface)/well surface.

2.12. Cytokine membrane antibody arrays

Cytokine assays were performed using the Proteome Profiler Human XL Cytokine Array kit (ARY022B; R&D Systems) according to the manufacturer's instructions. Membrane chemoluminescence was captured with the PXi imaging system (Syngene). Data acquisition and quantification were performed using Quick Spots Tool software (Western Vision Software).

2.13. Mouse experiments

Pancreatic cancer cells and PSCs orthotopic co-xenografting: Pancreatic cancer cells and PSCs were trypsinized, washed and resuspended in sterile PBS. A 1:3 mix of pancreatic cancer cells (10^6 MiaPaCa-2 cells) and PSCs shCTR or shFKBP7 (3×10^6) were co-injected in 50 µL of PBS, into the pancreas of anesthesized (Isoflurane, Isovet from Piramal Health) 8 week-old female Swiss Nude mice (Charles River, France). Tumor volumes were measured by ultrasound using the 3-dimensional reconstruction tool (Vevo 2100; VisualSonics), or using the following formula: tumor area * tumor diameter * (2/3) (Aixplorer; Supersonic imagine). Thirty-three days after injection, mice were euthanized and pancreata were removed and paraffin-embedded before being sliced and

stained. Mice were kept under specific pathogen-free conditions.

Pancreatitis induction: C57BL/6 mice were starved for 16h, subjected to 6 hourly intraperitoneal injections of 0.9 % sodium chloride (saline) or 50 μg/kg of cerulein (Sigma Aldrich), and sacrificed at 24h during the acute phase of pancreatitis.

Spontaneous tumors in mice: they were obtained using the KPC model (*Pdx-1-Cre; LSL-Kras$^{G12D/+}$; LSL-Trp53$^{R172H/+}$* [39]), as we previously published [40]. Pancreata were harvested, formalin-fixed and paraffin-embedded (FFPE).

All experiments were in accordance with institutional guidelines and European animal protection law and approved by the responsible government agency (Facility agreement number A31555010; Project number: AP AFIS#2l117-2019061900061441).

2.14. Bioinformatical and statistical analyses

PDX transcriptome analyses were obtained from processed dataset of the PaCaOmics clinical trial (NCT01692873) [41]. Laser microdissected stromal and epithelial compartments of RNAseq analyses from 65 PDAC patients were obtained from the gene omnibus database (GSE93326) [42]. Raw counts from RNA-Seq were normalized using the upper quartile normalization, after excluding genes in the Y chromosome locus, genes with fewer than 5 reads in 50 % of samples and genes with null variance in the dataset. P-values for comparisons were corrected as False Discovery Rate (FDR) using Bonferroni correction. Differentially expressed genes between the stromal and the epithelial compartments were expressed as Log2 fold-change (Log2FC) and considered significant if their adjusted p-value is below than 0.05. Gene annotation was performed using the function enrichGO from the R package *clusterProfiler*. Single cell datasets were obtained from Peng et al. [43]. Raw counts were log-normalized using the *Seurat* R package after exclusion of low-quality cells (<200 genes/cell and >4 % mitochondrial genes). To identify cell type clusters, PCA was performed using the most variable genes. Significant principle components were determined using JackStraw analysis on PCs 1 to 50. PCs 1 to 25 were used for graph-based clustering at res = 0.4. These groups were projected onto t-SNE analysis run using previously computed principle components 1 to 25. SCINA R package [44] with default parameters was used to distinguish cell types from single cell RNAseq. We used markers from MCPcounter [45] plus epithelial markers (KRT19, CDH1, MUC1, SOX9 and EPCAM). Fibroblastic populations have been subtracted with the use of *LUM, DCN, COL1A1, RGS5, ACTA2*, *PDGFRB* and *ADIRF* gene expression for further analyses, as performed in Ref. [43]. Pathway enrichment analyses for each cell were assessed using *GSVA* (gene set variation analysis) R package [46]. GSVA R package (V1.52.3) was used with default parameters. We applied published CAF and stromal PDAC subtype signatures to the fibroblastic populations in the single cell RNAseq. From GSVA we obtained a score (enrichment score) and no associated p-values as it is calculated from one sample and not a group of samples compared to another one. Pearson correlations between FKBP7 expression and GSVA results were computed.

All statistical analyses were performed using GraphPad Prism 9 software (GraphPad Software Inc., San Diego, USA). Number of animals and replicate *in vitro* experiments are specified in each figure legend. Results are presented as the mean ± SEM. Normal distribution of variables was computed using three complementary normality tests (D'Agostino-Pearson, Shapiro-Wilk and Anderson-Darling), as suggested by the Prism Statistics Guide (www.graphpad.com/guides/prism/latest/statistics/stat_choosing_a_normality_test.htm), to infer "non-normality" of the distribution of our data sets if at least one test says so. Comparison of a continuous variable in two or more than two groups with normal distribution was performed using parametric test, *i.e.*, *t*-test or ANOVA, respectively, with a Bonferroni post-test for multi-parametric analyses. If the variable was not normally distributed, a non-parametric test, *i.e.*, Mann-Whitney or Kruskal-Wallis, was applied for comparison in two or more than two groups, respectively, with a Dunns post-test for multi-parametric analyses. All p-values were two-sided, and $P < 0.05$ was considered statistically significant.

3. Results

3.1. Identification of FKBP7 as an ER-resident protein specifically overexpressed in human PSCs and CAFs as compared to tumor cells

To compare protein synthesis on cytosolic versus ER-bound ribosomes, a SUnSET assay [37] was performed on fractionated protein extracts from two pancreatic tumor cell lines (MiaPaCa-2, Panc-1) and from immortalized PSCs and CAFs. In PSCs and CAFs, puromycin incorporation was consistently higher in the membranous (organelles) fraction than in the cytosolic fraction, which are enriched in ER-resident PERK and cytosolic eIF4E-BP1 proteins, respectively (Fig. 1A–S1A). In contrast, tumor cell lines showed the opposite pattern, but with a more balanced ratio of puromycin incorporation between both cell compartments, as quantified (Fig. S1B). The elevated protein synthesis at ER-bound ribosomes in PSCs and CAFs also correlated with higher basal ER stress, as indicated by increased ATF4 expression and a higher p-eIF2α/total eIF2α ratio in untreated (UT) cells, compared to tumor cells (Fig. 1B). While PSCs and CAFs displayed similar ER stress responses to thapsigargin or brefeldin-A —a non-competitive inhibitor of ER Ca2+ ATPase that depletes ER calcium stores, or an inhibitor of protein transport from the ER to the Golgi, respectively—compared to tumor cells, the outcomes were different. Under induced ER stress, PSCs and CAFs showed reduced apoptotic cell death and increased survival, measured by PARP cleavage and MTT assays, respectively (Fig. 1B–C, S1C). This suggests an optimized ER stress response in PSCs and CAFs, likely to support their high protein folding demand.

To identify stroma-specific ER proteins contributing to this resilience, we screened for ER-related genes in two PDAC RNAseq databases: patient-derived xenografts [41], and tissue microdissected lesions [42], where stromal and tumor epithelial gene expression are separately quantified. We found 7 and 4 upregulated genes (Log2FC > 1) among chaperones and co-chaperones in the stromal compartment *versus* the tumor epithelium, respectively of [41] (Table 1) or of [42] (Table 2), with FKBP7 mRNA showing the highest fold-change among stromal-enriched genes (Fig. 1D).

Immunohistochemistry on PDX tumors confirmed high FKBP7 protein levels in stromal areas negative for CK19 (tumor epithelial marker) (Fig. 1E–S1D). Western blots further showed high FKBP7 levels in PSC and CAF cultures expressing fibroblast markers (e.g., αSMA, FAPα, type I collagen, periostin), but not in cancer cells (Fig. 1F) [47]. Single-cell RNAseq analysis from Peng et al. [43] supported these findings, indicating FKBP7 is predominantly expressed in fibroblast populations (Fig. 1G–H), where cluster numbers 4, 5, 11 and 12 co-express at least one of the previously described fibroblast markers (LUM, DCN, COL1A1, ACTA2, FAP, POSTN, PDPN, PDGFRA, ISLR, and LRRC15) (Fig. S1E); similarly as those markers, the percentage of fibroblasts expressing FKBP7, and expression level, are higher in the tumor compared to normal adjacent tissue (Fig. S1F). Additionally, murine PDAC tissue (KPC tumors, *Pdx-1-Cre; LSL-Kras$^{G12D/+}$; LSL-Trp53$^{R172H/+}$* [39]) showed FKBP7 expression in the stroma but not in adjacent CK19-positive tumor glands (Fig. S1G).

Given the heterogeneity of FKBP7 expression across PSC and CAF cell lines (Fig. 1F) and within single-cell data (Fig. 1H, S1E-F), we examined whether stromal FKBP7 expression correlates with clinical outcomes in PDAC patients. In a tissue microarray of 27 PDAC tumors, high FKBP7 expression in the stroma, as assessed by immunohistochemistry (Fig. 1I), was significantly associated with improved overall survival (Fig. 1J) and nearly with progression-free survival (Fig. S1H).

Collectively, these results establish that FKBP7 is primarily expressed in PSCs and CAFs and that its elevated stromal expression correlates with a better prognosis in PDAC patients.

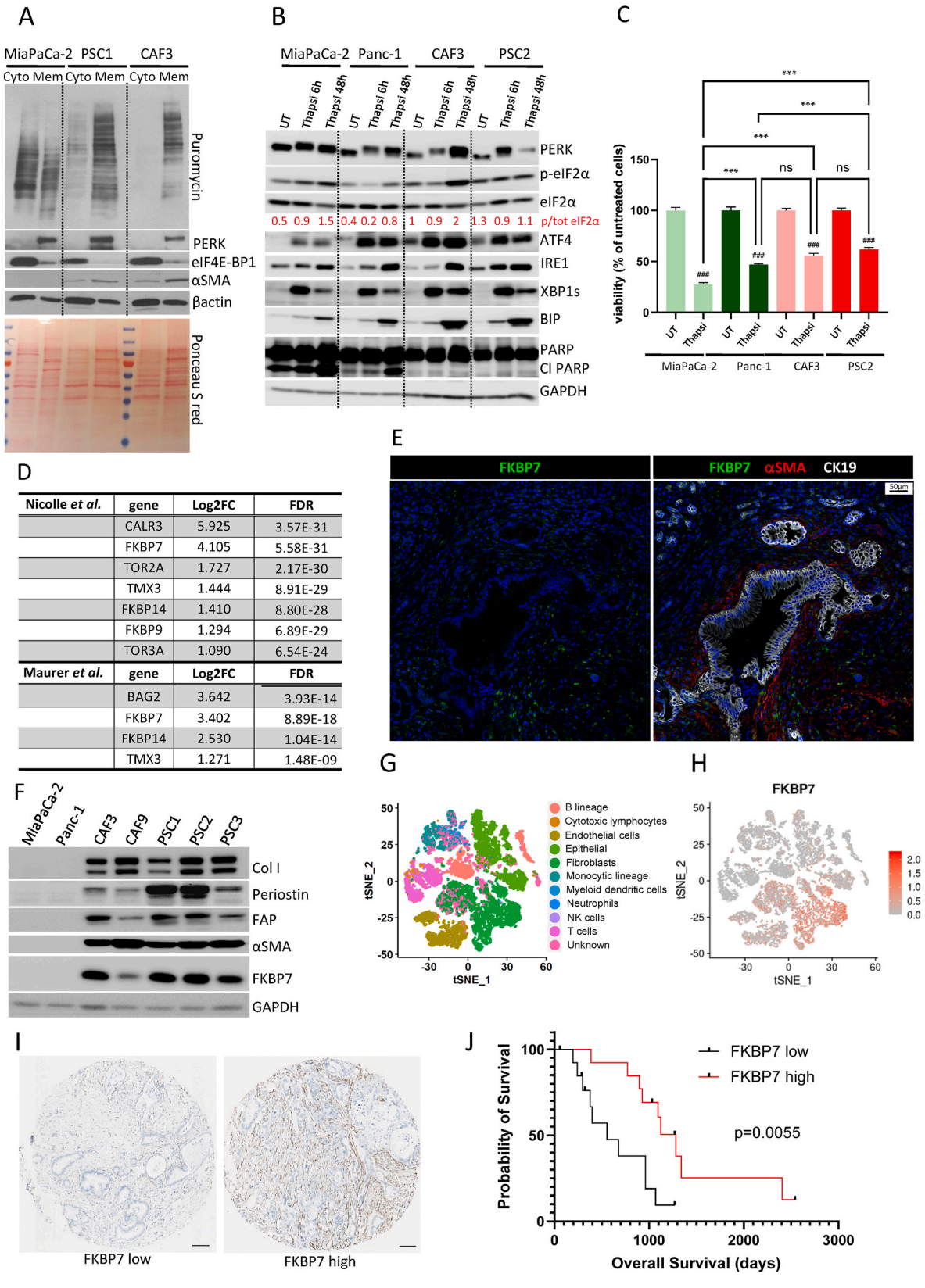

(caption on next page)

Fig. 1. PSCs and CAFs are resistant to ER stress as compared to tumor cells, and overexpress the ER co-chaperone FKBP7.
A- Representative Western blots showing SunSET assay after subcellular fractionation (cyto: cytosol; mem: membranes) of tumor cells, PSC1 and CAF3, with PERK, eIF4E-BP1, αSMA and puromycin antibody. Ponceau S red staining serves as loading control. N = 3 experiments. **B-** Representative Western blots of tumor cells (MiaPaCa-2 and Panc-1), CAF3 and PSC2 treated or not (UT) with thapsigargin (3 μM) for the indicated times, with PERK, p-eIF2α, eIF2α, quantified ratio of p-eIF2α/total eIF2α, ATF4, IRE1, XBP1s, BiP, PARP and Cleaved (Cl) PARP antibody. GAPDH antibody serves as a loading control. N = 3 experiments. **C-** Viability of tumor cells (MiaPaCa-2 and Panc-1), CAF3 and PSC2 treated or not (UT) for 48h with thapsigargin (3 μM) was assessed by MTT. Results (mean, SEM) are presented for each cell type. (N = 3) ANOVA was used to generate p values, ***$p < 0.001$, ns. non significant. **D-** Differential expression of (co)-chaperone mRNAs (expressed as Log2FC) in stromal *versus* tumor epithelial compartments of the Nicolle et al. (patient-derived xenografts) [41] and Maurer et al. (patient tumors) [42] cohorts. **E-** Representative images of immunohistofluorescence co-staining of CK19, FKBP7 and αSMA in sections of human PDAC patient tissues. **F-** Representative Western blots of tumor cells (MiaPaCa-2, Panc-1), two different CAFs and three PSCs with type I collagen (ColI), Periostin, FAP, αSMA and FKBP7 antibodies. GAPDH antibody serves as a loading control. N = 3 experiments. **G-** Plot of the different cell types onto the t-SNE map from single cell RNA sequencing [43]). Fibroblasts are highlighted in green. **H-** Plot of expression levels of FKBP7 in each analyzed cell (all cell types, Peng et al.) onto the t-SNE map or as a heatmap. Color key from light to dark red indicates relative expression levels from low to high. **I-** Representative images of immunohistochemistry staining of FKBP7 on two patient PDAC tissues extracted from a 27-patient tissue-microarray analysis, and showing low or high FKBP7 expression. **J-** Kaplain-Meier plot showing overall survival of 27 PDAC patients (each patient IHC is performed in sextuplicate), and split based on the median expression of FKBP7 quantified by immunohistochemistry using an anti-FKBP7 antibody and a tissue-microarray comprising 6 spots for each patient tumor. A Log-rank (Mantel-Cox) test was used to generate p-value.

3.2. FKBP7 expression is upregulated by stiffness- and TGFβ-triggered signals

We examined FKBP7 expression by immunohistochemistry in patient and murine pancreatic lesions. In patients, FKBP7 is expressed in the stroma around early acinar-to-ductal metaplasia (ADM) and PanIN lesions, found at a distance from PDAC tissue, but not in healthy exocrine tissue (Fig. 2A, S2A). Unlike FKBP7, αSMA, an early TGFβ-induced marker of activated PSCs, does not appear in tumor-distant stroma adjacent to ADM lesions, except faintly in fibroblasts comprised in the interlobular space; αSMA is also weakly expressed in a thin stromal layer near PanIN lesions and in vascular smooth muscle in healthy tissue (Fig. 2A). In human chronic pancreatitis, FKBP7 and αSMA immunostaining show good expression of FKBP7 but very weak expression of αSMA, in the stroma around acinar lesions, whereas αSMA is well expressed around vessels (Fig. S2B). In mice, FKBP7 is absent in healthy pancreas, where αSMA stains only blood vessels (Fig. S2C). However, in acute pancreatitis lesions (induced by caerulein injection), both FKBP7 and αSMA are present in the stroma, accompanied by abundant CD45-positive inflammatory cells (Fig. S2C).

To explore FKBP7 expression regulation, we tested signals that occur early during pancreatic tumorigenesis, i.e. tissue stiffening and TGFβ secretion and activation. We cultured immortalized PSCs with or without TGFβ for up to 48 h. FKBP7 showed basal expression in two PSC lines, which increased slightly over time alongside type I collagen expression and FAK phosphorylation (Fig. 2B–S2D). On high-stiffness plastic, TGFβ did not alter FKBP7 levels but significantly increased Smad2 and FAK phosphorylation, as well as αSMA, type I collagen, and CTGF expression, as expected (Fig. 2B–S2D).

Since plastic culture mimics high-stiffness conditions, we tested if FKBP7 is responsive to mechanical stimulus by culturing PSCs on low- (0.5 kPa) and high- (32 kPa) stiffness dishes, with or without TGFβ. FKBP7, αSMA, type I collagen, and FAK phosphorylation were elevated on high-stiffness or plastic compared to low-stiffness conditions; FAK inhibition reduced these levels. On low-stiffness, TGFβ increased FKBP7 expression, as well as Smad2 phosphorylation, αSMA, and type I collagen (Fig. 2C). A similar TGFβ-induced gene expression pattern, including FKBP7, was observed in MEFs on low-stiffness dishes (Fig. 2D).

Overall, these findings suggest FKBP7 is an early marker of PSC activation in chronic pancreatitis or pancreatic cancer. Its expression aligns with pro-fibrogenic signals from matrix stiffening or TGFβ treatment and depends on FAK activity.

3.3. FKBP7 inhibits PSC contractility

Given FKBP7 association with better PDAC prognosis, we tested its role in PSCs by altering FKBP7 expression through lentiviral knockdown (shRNA FKBP7, FKBP7^{KD}) or overexpression (ploc FKBP7, FKBP7^{OE}) in three PSC lines with varying basal FKBP7 levels (Fig. 1F). Scanning electron microscopy showed that control PSCs (shCTR cells, expressing FKBP7) spread out with a crisscrossed cytoskeletal network, likely actin fibers. In contrast, FKBP7^{KD} PSC were stretched, displaying well-aligned fibers along the cell axis (Fig. S3A). Confocal imaging, using phalloidin labelling of actin, p-FAK and αSMA antibodies, revealed that both shCTR and FKBP7^{KD} PSCs contain αSMA but with different actin organization, as well as different p-FAK cellular distribution. ShCTR PSCs displayed transverse and dorsal fibers at lamellipodia, while FKBP7^{KD} PSCs had long ventral stress fibers that branch at each end with large p-FAK-positive focal adhesions rich in p-MLC2 (Fig. 3A–S3B).

FKBP7^{OE} PSCs showed fewer αSMA stress fibers associated with p-FAK-positive focal adhesions, than mock PSCs (ploc CTR) (Fig. 3B). This was confirmed by fluorescence signal quantification (Figs. S3C–D, left panels): higher FKBP7 expression in FKBP7^{OE} PSCs reduced per-cell αSMA fluorescence, indicating fewer αSMA-activated PSCs in FKBP7^{OE} compared to mock PSCs (Figs. S3C–D). High-content screening further showed that mock PSCs had larger and longer αSMA fibers, indicative of contractile fibers, compared to FKBP7^{OE} cells (Figs. S3C–D). Consistently, lower FKBP7 expression, with more stress actin fibers in PSCs FKBP7^{KD} and mock PSCs compared to shCTR and FKBP7^{OE} PSCs, respectively, correlated with increased cell contractility in a collagen gel contraction assay (Fig. 3C).

Moreover, FKBP7^{OE} PSCs showed reduced stiffness-induced activation, evidenced by lower, compared to mock PSCs, FAK phosphorylation and αSMA expression on stiff matrices (32 kPa or plastic), though TGFβ treatment on soft matrix (0.5 kPa) had the same outcomes in FKBP7^{OE} and mock PSCs (Fig. 3D). These results suggest FKBP7 in PSCs inhibits the acquisition of a contractile fibroblast-activated phenotype, specifically when triggered by matrix stiffening and FAK-dependent stress fiber formation.

3.4. FKBP7 modulates PSC secretome and restrains in vivo pancreatic tumor growth

To investigate FKBP7 role in preventing a pro-tumoral activated fibroblastic phenotype, we analyzed the secretome of control PSC (shCTR) and two FKBP7^{KD} PSC lines (shFKBP7- shRNA1 and shFKBP7-shRNA2) using cytokine arrays (Fig. S4A). FKBP7 knockdown led to 52 downregulated and 30 upregulated proteins, with 26 common downregulated and 20 common upregulated across both FKBP7^{KD} lines (Fig. 4A–S4A). Notably, FKBP7 knockdown induced a switch to an inflammatory state, increasing secretion of cytokines like IL-6, IL-23, LIF, IL-8, and LCN2, which are linked to a STAT3-centered network (Fig. 4A–S4B, String interactome prediction). Conversely, proteins like thrombospondin-1 (TSP1) were downregulated (Fig. 4A). We confirmed TSP1 downregulation and IL-6 upregulation in FKBP7^{KD} PSC protein lysates and conditioned media, with FKBP7 rescue (FKBP7^{OE}, overexpressing FKBP7 in FKBP7^{KD} cells) reversing these changes (Fig. 4B–E).

Table 1
Comparison of expression of ER-related genes in PDX tumor epithelium *versus* stroma.

gene	Log2FC	FDR
PENK	−13.806	6.72E-32
FCGR2B	−13.527	1.11E-31
ADAMTS5	−12.535	4.15E-32
IGF1	−11.623	3.68E-31
TRDN	−11.426	5.12E-19
COL11A1	−11.243	1.32E-31
COL10A1	−10.804	6.04E-30
PRSS57	−10.787	4.71E-32
COL15A1	−10.622	4.88E-31
APOE	−10.452	4.89E-31
COL3A1	−10.140	4.89E-31
HK3	−9.884	4.51E-31
F13A1	−9.707	1.73E-31
COL26A1	−9.621	2.40E-27
DCSTAMP	−9.374	9.88E-34
SPARC	−9.331	4.89E-31
CCR5	−9.246	3.68E-31
COL14A1	−9.073	5.05E-31
COL1A2	−8.940	4.89E-31
COL23A1	−8.883	4.78E-31
FBN1	−8.861	4.89E-31
COL8A1	−8.802	5.30E-31
SPARCL1	−8.771	4.89E-31
HGF	−8.116	8.32E-32
IL27	−8.111	1.47E-32
COL5A1	−8.087	4.70E-31
COL5A2	−8.063	4.89E-31
PRTN3	−7.913	2.03E-32
DOCK2	−7.877	3.79E-31
SYT6	−7.844	2.87E-29
ARG1	−7.819	8.06E-31
ISLR	−7.811	2.06E-31
COL6A3	−7.797	4.89E-31
THBS4	−7.761	5.05E-31
MMP8	−7.694	2.05E-31
COL1A1	−7.468	4.89E-31
CACNA1G	−7.450	5.05E-31
HLA-DQA1	−7.445	1.24E-30
IGFBP5	−7.443	7.71E-31
ARHGAP9	−7.439	4.89E-31
COL4A1	−7.307	4.89E-31
FGR	−7.293	4.88E-31
MAN1C1	−7.201	4.89E-31
CASQ1	−7.075	5.40E-31
CFP	−7.009	4.89E-31
COL5A3	−7.007	4.89E-31
WNT5A	−6.993	5.61E-31
CASQ2	−6.895	4.50E-30
TIMP3	−6.757	5.57E-31
COL8A2	−6.471	1.72E-30
COL12A1	−6.430	5.78E-31
SPP1	−6.273	7.35E-31
TGFB3	−6.195	5.05E-31
FMO1	−6.162	9.55E-30
DMP1	−6.135	2.92E-31
EBI3	−6.105	4.51E-31
SERPING1	−6.070	4.89E-31
TNC	−6.061	8.90E-31
CALR3	−5.926	3.57E-31
CLEC3B	−5.792	1.15E-28
VWF	−5.714	6.82E-31
COL4A2	−5.709	4.89E-31
CTSG	−5.678	3.76E-27
IGFBP7	−5.655	5.05E-31
COL6A2	−5.654	4.88E-31
HLA-DQB1	−5.566	2.25E-30
FASLG	−5.469	1.41E-25
ACTN2	−5.369	2.04E-12
BIN2	−5.298	4.89E-31
CTSW	−5.260	3.81E-30
SYT3	−5.241	9.71E-31
F2RL3	−5.204	5.27E-30
FN1	−5.186	5.30E-30

Table 1 (*continued*)

gene	Log2FC	FDR
ARSI	−5.169	1.28E-30
PTX3	−5.125	1.21E-29
RARRES2	−5.116	7.79E-31
NKD2	−5.115	1.42E-30
COL20A1	−4.999	1.09E-30
ABCA1	−4.996	4.89E-31
P4HA3	−4.957	8.33E-31
DLC1	−4.957	4.88E-31
F7	−4.926	7.55E-29
FSTL1	−4.701	1.02E-30
SDC2	−4.694	3.82E-29
CRYAB	−4.690	5.47E-30
ADAMTSL1	−4.665	7.81E-30
SPON1	−4.649	1.02E-29
GRIA1	−4.615	1.94E-19
MMRN1	−4.598	4.20E-18
PGLYRP1	−4.561	4.89E-31
ARSB	−4.443	4.89E-31
PF4	−4.440	5.12E-30
GPX7	−4.427	6.88E-31
BCL2	−4.383	5.05E-31
THBS1	−4.319	7.35E-30
CRISPLD2	−4.246	1.46E-30
CHRDL1	−4.236	1.26E-28
IL12B	−4.171	1.52E-28
FKBP7	−4.106	5.59E-31
COL24A1	−4.100	3.17E-29
ADAMTS7	−4.000	6.17E-31
ELANE	−3.950	6.76E-12
KDELC1	−3.935	4.89E-31
IGFBP4	−3.925	5.23E-31
KNG1	−3.920	3.30E-28
CSF1	−3.870	7.11E-30
GRP	−3.866	3.60E-14
OTOR	−3.830	6.13E-16
CFD	−3.824	0.02477241
SERPINH1	−3.719	4.89E-31
GAS6	−3.702	5.23E-31
LGALS1	−3.660	1.12E-29
SYT4	−3.645	6.30E-29
SYT15	−3.606	2.25E-30
VEGFC	−3.587	1.61E-27
GMFG	−3.559	2.33E-27
F2R	−3.513	8.94E-30
SERPINE1	−3.478	4.99E-28
DPYSL3	−3.430	2.04E-30
COL6A1	−3.426	1.09E-29
FABP5	−3.390	2.09E-29
GPC3	−3.317	4.83E-28
PCSK2	−3.304	4.9279E-05
CD74	−3.240	1.17E-26
DOC2B	−3.205	9.57E-28
ASGR2	−3.172	3.02E-28
MPO	−3.032	3.34E-21
SLC37A2	−3.014	1.99E-27
MAN2B1	−3.008	4.89E-31
BACE1	−3.008	1.42E-30
NPC2	−2.976	3.34E-30
RYR1	−2.965	4.32E-08
F10	−2.962	1.71E-25
MFGE8	−2.925	1.73E-30
COL18A1	−2.903	9.86E-30
HPSE	−2.876	1.16E-30
COL19A1	−2.858	0.00187238
TF	−2.770	9.55E-30
PROS1	−2.692	5.59E-31
KCTD17	−2.691	5.78E-31
PDGFD	−2.663	8.96E-28
LRRK2	−2.640	1.52E-27
COL25A1	−2.620	1.68E-22
COPG2	−2.616	4.89E-31
TXNDC16	−2.604	6.17E-31
ITPR1	−2.586	2.11E-28
GM2A	−2.560	1.20E-29
C3	−2.557	2.48E-23
CYR61	−2.554	2.56E-28

(*continued on next page*)

Table 1 (*continued*)

gene	Log2FC	FDR
HLA-DRB5	−2.545	7.47E-18
MAN1A1	−2.535	1.05E-29
CTSD	−2.500	8.63E-29
TIMP2	−2.445	2.84E-30
IGFBP3	−2.377	5.50E-25
LIN28A	−2.377	1.64E-07
FAM20C	−2.359	2.10E-26
RAB3A	−2.336	2.53E-29
COL16A1	−2.309	2.56E-27
HIST1H4A	−2.306	2.47E-15
POMC	−2.305	1.11E-29
APOOL	−2.279	4.89E-31
PKD2	−2.275	1.12E-29
MXRA8	−2.269	3.00E-28
COL13A1	−2.249	1.21E-21
ARSK	−2.201	2.66E-30
CALU	−2.198	5.23E-31
GUSB	−2.168	5.78E-31
TGFB1	−2.149	1.33E-30
CTSA	−2.124	1.37E-30
HIST2H3A	−2.110	0.00030948
GPX8	−2.110	5.48E-28
PRSS23	−2.105	3.52E-28
SERPINC1	−2.053	7.45E-26
FERMT3	−2.048	1.26E-24
COL11A2	−2.041	1.46E-27
HIST1H3A	−1.996	2.30E-14
RPH3A	−1.954	1.60E-15
HEXB	−1.923	1.98E-28
S100A8	−1.908	1.57E-26
SYT11	−1.893	1.06E-22
GRN	−1.879	5.40E-31
OSTF1	−1.861	4.89E-31
FBXO6	−1.836	1.23E-28
HLA-G	−1.788	2.22E-21
APOA2	−1.756	2.44E-17
TOR2A	−1.727	2.18E-30
VAT1	−1.718	8.91E-29
CST3	−1.717	2.48E-28
RTN1	−1.708	9.04E-21
STX5	−1.661	1.20E-30
CAMP	−1.645	2.89E-11
CTSZ	−1.625	9.82E-29
ANAPC1	−1.593	4.89E-31
CACNA1H	−1.580	2.71E-17
PTPN6	−1.566	9.21E-29
LAMB1	−1.545	6.31E-27
CTSC	−1.539	2.03E-24
CKAP4	−1.533	4.39E-29
EPHA5	−1.523	1.0828E-05
SPPL2A	−1.507	2.84E-30
CREB3L2	−1.501	4.25E-28
LMAN1L	−1.493	2.06E-11
FTL	−1.491	1.52E-25
EHMT2	−1.484	4.89E-31
SERPINA3	−1.461	1.62E-17
GNS	−1.452	1.77E-29
TMX3	−1.445	8.91E-29
CREB3L3	−1.431	2.68E-18
ARSA	−1.427	2.49E-30
SGPL1	−1.417	7.12E-29
FKBP14	−1.411	8.80E-28
GOSR2	−1.391	5.05E-31
SCG3	−1.345	3.74E-18
RAP1GDS1	−1.342	5.59E-31
AMPD3	−1.338	3.81E-23
PRKCD	−1.334	3.53E-26
GALNS	−1.320	2.91E-28
KCNB1	−1.308	7.95E-19
SCAMP5	−1.305	1.51E-21
FKBP9	−1.295	6.89E-29
GLA	−1.284	6.77E-22
TUSC3	−1.270	3.92E-14
ITIH3	−1.269	2.05E-19
MAPK7	−1.269	3.30E-28
ATF3	−1.257	1.30E-14

Table 1 (*continued*)

gene	Log2FC	FDR
HFE	−1.252	1.76E-27
PDGFC	−1.249	1.46E-19
HIST1H2BB	−1.246	0.00238364
FUCA1	−1.241	1.37E-26
FITM1	−1.240	0.0020121
FAM129A	−1.239	7.58E-21
MZB1	−1.233	0.00017533
LYZ	−1.231	1.43E-17
REEP2	−1.230	6.02E-25
COTL1	−1.227	3.76E-24
HLA-A	−1.225	5.09E-20
TBC1D20	−1.217	5.05E-31
LAMC1	−1.216	5.67E-25
ANAPC2	−1.214	4.89E-31
EXT1	−1.205	1.80E-26
CREG1	−1.204	3.10E-22
SSR3	−1.190	3.00E-28
PDGFB	−1.177	3.54E-19
EVA1A	−1.150	4.99E-17
TRAM2	−1.133	5.18E-24
XXYLT1	−1.129	1.02E-25
ELOVL4	−1.128	6.40E-11
HGFAC	−1.114	1.49E-15
POGLUT1	−1.103	5.66E-30
PTPN1	−1.102	8.01E-28
GYG1	−1.091	3.17E-16
TOR3A	−1.091	6.54E-24
CDKN2B	−1.068	3.74E-10
CLN8	−1.048	2.10E-21
FKBP10	−1.035	6.30E-13
SLC35B4	−1.032	2.37E-26
CPPED1	−1.026	2.62E-21
CDKN2D	−1.023	1.30E-22
TMEM132A	−1.021	2.21E-15
PADI2	−1.017	8.62E-13
SAMD8	−1.014	1.42E-24
NUCB1	−1.008	5.15E-28
PLG	−1.002	1.95E-06
LRAT	1.006	0.03611232
GOLGB1	1.011	3.84E-27
PDCD6	1.022	7.36E-27
CREB3L1	1.034	1.0748E-05
GHDC	1.039	5.49E-24
UFM1	1.041	1.99E-25
CEBPB	1.060	2.89E-14
FOS	1.065	1.36E-15
ANAPC7	1.068	6.70E-26
PARK7	1.075	9.98E-25
INSIG1	1.083	6.91E-15
TMBIM6	1.092	4.39E-28
DAB2IP	1.102	1.01E-19
TMCO1	1.105	1.69E-26
SRP14	1.106	3.28E-27
CSTB	1.108	6.76E-15
FOXRED2	1.127	7.77E-14
EIF2B5	1.133	5.40E-31
TFG	1.143	5.05E-31
ZC3H12A	1.147	6.62E-21
NPLOC4	1.149	3.74E-29
VEGFB	1.151	1.34E-20
CA4	1.168	8.99E-14
APLP2	1.174	1.45E-22
FRK	1.174	4.54E-18
CEP290	1.179	3.88E-22
TMED4	1.181	4.89E-31
PDXK	1.181	4.45E-20
MAP3K5	1.182	5.64E-19
PA2G4	1.212	1.05E-29
DAG1	1.215	9.45E-22
TRAM1	1.233	8.54E-26
ATL2	1.260	3.52E-28
PCYOX1L	1.262	3.94E-12
CAV2	1.263	6.14E-12
H2AFX	1.273	9.19E-22
PPIE	1.296	6.71E-27
MPPE1	1.321	1.51E-24

(*continued on next page*)

Table 1 (*continued*)

gene	Log2FC	FDR
DBI	1.326	2.48E-27
UBAC2	1.342	5.68E-29
EDEM3	1.344	1.39E-15
DERA	1.349	2.33E-27
ADAMTSL4	1.360	2.7914E-05
BCAP31	1.374	8.94E-30
ARL6IP1	1.388	1.19E-28
OLA1	1.396	4.89E-31
SYT14	1.404	0.00049219
NIT2	1.445	6.82E-31
CASP4	1.456	5.47E-30
IMPDH2	1.457	3.62E-25
DERL3	1.464	8.42E-11
QPCT	1.472	0.00165744
DGAT2	1.477	4.32E-16
GPAA1	1.478	5.33E-29
THADA	1.506	5.05E-31
CES1	1.546	0.00024184
MBOAT4	1.548	5.25E-08
ANXA2	1.553	3.81E-30
FAM3C	1.557	1.52E-23
SYTL3	1.582	9.07E-15
MARCH6	1.597	1.83E-29
ACTN4	1.599	1.24E-29
TUBB4B	1.606	1.46E-30
DHCR7	1.623	1.24E-27
ANAPC16	1.629	1.12E-30
GET4	1.643	9.24E-30
SGMS2	1.664	2.38E-25
PNPLA2	1.673	1.64E-26
PCSK1	1.678	1.66E-12
AHSG	1.690	4.11E-12
TMED2	1.706	4.89E-31
STX1A	1.709	5.03E-25
LBR	1.716	1.19E-28
RAB37	1.731	7.6455E-05
PPP1R15A	1.734	2.11E-28
ANKLE2	1.761	1.12E-30
MVP	1.767	8.90E-31
CHIT1	1.768	7.6998E-05
CACNA1I	1.769	0.00080609
RAB27A	1.786	5.68E-23
CAPN2	1.794	5.97E-31
CATSPER2	1.836	5.18E-24
GCC2	1.847	5.68E-29
TMEM97	1.855	7.28E-28
EIF2AK1	1.876	4.89E-31
SCCPDH	1.879	3.00E-28
LEFTY2	1.881	3.9228E-05
BGLAP	1.888	1.41E-22
SORL1	1.892	3.60E-20
DSN1	1.911	4.89E-31
ILF2	1.927	4.89E-31
SPPL2B	1.944	1.12E-29
LIPC	2.004	0.00443379
F2	2.014	2.03E-06
TRIB3	2.050	1.61E-18
HIST1H2AB	2.071	2.25E-10
HLA-E	2.077	7.28E-28
GHRL	2.104	2.75E-25
PTGES2	2.116	3.34E-30
RNF103	2.127	5.15E-28
TRIM13	2.148	4.89E-31
ASPH	2.168	2.11E-30
QSOX1	2.171	1.06E-25
DNAJB1	2.175	5.05E-31
NHLRC2	2.184	7.05E-31
ARSJ	2.196	6.27E-21
GOLM1	2.205	8.80E-26
COL9A3	2.207	5.7239E-05
HSPH1	2.209	1.02E-30
HIST1H2BL	2.231	2.63E-19
VEGFA	2.232	2.45E-26
SLC37A4	2.241	5.23E-31
NOL3	2.246	8.94E-30
CAPN1	2.253	4.89E-31

Table 1 (*continued*)

gene	Log2FC	FDR
MATN3	2.265	1.08E-15
ALDOC	2.268	1.56E-24
GBA2	2.309	4.89E-31
ITIH4	2.316	1.25E-22
ALOX5	2.368	8.62E-13
CLU	2.385	0.01791219
OSBPL3	2.501	1.79E-30
GCA	2.574	5.30E-30
TMEM117	2.579	1.99E-27
OSCAR	2.587	1.15E-09
OSBPL7	2.592	1.87E-27
RYR3	2.596	1.93E-27
ARV1	2.642	4.89E-31
SYTL4	2.735	1.28E-27
TM6SF2	2.751	4.60E-07
SVIP	2.760	5.97E-31
ABCB9	2.780	4.89E-31
PIGG	2.797	4.89E-31
SUMF2	2.814	4.89E-31
PYGB	2.829	6.38E-31
HIST1H2BC	2.867	1.85E-20
SYTL2	2.947	2.21E-23
DBH	2.973	1.80E-07
HSP90AA1	3.065	4.89E-31
DNAJB2	3.097	4.89E-31
DHRS9	3.108	6.19E-07
SYT17	3.111	3.30E-28
SYT13	3.204	5.48E-21
CD55	3.226	8.53E-28
UNC13D	3.235	1.05E-29
ELOVL6	3.277	7.29E-31
YOD1	3.280	4.89E-31
UBC	3.313	4.89E-31
COL4A3	3.325	0.00215237
HIST3H2BB	3.371	5.71E-24
HEBP2	3.382	4.89E-31
PDIA2	3.407	2.57E-19
GSTP1	3.424	5.05E-31
SERPINB1	3.466	2.74E-30
HIST1H2AD	3.577	6.84E-19
HIST1H2BO	3.608	3.06E-24
RNASET2	3.626	1.86E-28
DYNLT1	3.639	4.89E-31
SYT16	3.653	3.83E-11
SYT7	3.655	9.60E-17
TTC23L	3.719	1.04E-27
JUP	3.723	9.55E-30
SRP9	3.812	4.89E-31
IGF2	3.856	0.00025444
HSPA1L	3.939	1.41E-29
F8	3.944	1.08E-10
SERPINF2	3.960	1.90E-26
SLC37A1	3.967	3.94E-30
TMEM30B	3.988	1.49E-28
TMEM170A	4.010	4.89E-31
XRCC6	4.046	4.89E-31
COL4A4	4.056	4.97E-16
MAPK10	4.074	3.25E-12
SLPI	4.084	1.17E-26
F5	4.100	5.89E-22
BRSK2	4.128	8.71E-28
LRRC7	4.164	3.51E-30
BMP4	4.237	1.02E-25
ITIH2	4.288	1.42E-15
AREG	4.318	4.88E-27
SYT2	4.357	5.28E-31
CDA	4.366	8.46E-22
SEC31B	4.482	4.89E-31
COL4A6	4.536	0.0205178
A1BG	4.548	7.97E-28
COL9A2	4.631	4.25E-28
COL9A1	4.712	8.83E-16
FGA	4.719	1.61E-08
ATG10	4.771	4.89E-31
TH	4.777	3.37E-18
RYR2	4.780	4.50E-18

(*continued on next page*)

Table 1 (*continued*)

gene	Log2FC	FDR
BPI	4.796	0.00014809
SERPINA1	4.834	1.56E-24
FOLR1	4.938	2.03E-14
COL22A1	4.945	5.99E-17
SRP54	4.960	4.89E-31
CDK6	4.989	1.42E-30
TRPV6	5.009	1.92E-18
WNT7B	5.203	8.80E-28
XRCC5	5.214	4.89E-31
ADAMTS13	5.216	4.83E-31
HLA-F	5.314	4.80E-30
SYT1	5.334	1.60E-12
TMED6	5.580	7.01E-32
SYTL1	5.625	7.83E-27
TGFA	5.787	5.40E-31
TC2N	5.815	3.99E-29
FBXO2	5.831	1.41E-26
FGG	5.873	3.8073E-05
PCSK9	5.931	4.50E-29
APOA1	5.965	6.64E-17
SLC27A5	6.033	4.86E-31
C2CD4A	6.039	2.13E-26
LCN2	6.181	2.12E-27
SYT8	6.255	1.02E-29
IL23A	6.284	3.46E-31
ELOVL7	6.320	1.37E-30
C2CD4D	6.320	7.97E-33
TMEM27	6.433	1.88E-28
LAMP5	6.489	1.02E-21
CNIH3	6.498	3.39E-32
PROM1	6.664	8.08E-27
SYTL5	6.787	2.58E-28
HIST1H2BN	6.820	6.21E-32
WNT3	7.072	6.00E-32
APOB	7.598	4.06E-11
F12	7.799	2.18E-31
ALB	7.821	9.52E-14
RBX1	7.854	4.89E-31
PTGDS	7.937	7.36E-23
GJB2	7.974	6.81E-31
SHH	8.208	6.25E-31
SGPP2	8.230	8.61E-31
MSLN	8.424	2.64E-29
CD59	8.534	4.89E-31
HIST1H2BD	8.597	1.92E-31
SLC27A2	8.608	1.58E-30
MIA	8.961	3.60E-30
OLFM4	9.108	3.35E-18
WNT7A	9.625	1.18E-26
IGFBP1	10.243	6.86E-30
HIST1H2BK	10.405	2.18E-31
AOC1	10.520	3.32E-30
UBA52	11.119	4.86E-31
AGR2	15.964	1.55E-31

STAT3 phosphorylation, which increased in FKBP7^{KD} cells, decreased upon FKBP7 rescue (Fig. 4D), aligning with the prediction that FKBP7 knockdown upregulates STAT3-activating cytokines (Fig. S4A). Further bioinformatics analysis of Peng et al. pancreatic single-cell RNAseq data [43] revealed a negative correlation between FKBP7 expression and both the "activated inflammatory stroma" signature of Puleo et al. [48], and the "CAF IL6/LIF" signature of Dominguez et al. [49] (Fig. S4C), consistent with the inflammatory profile, IL-6 secretion, and STAT3 activation seen in FKBP7^{KD} PSC (Fig. 4A–C).

To evaluate the impact of FKBP7 on pro-tumor functions in PSCs, we xenografted MiaPaCa-2 pancreatic cancer cells with either control PSCs (shCTR) or FKBP7^{KD} PSCs (two FKBP7-targeting shRNA lines) into the pancreas of nude mice, monitoring tumor growth (Fig. 4F). By day 33, co-xenografts with FKBP7^{KD} PSCs produced larger tumors compared to those with FKBP7-expressing control PSCs (shCTR) (Fig. 4F). This result indicates that the activated PSC phenotype observed *in vitro* following FKBP7 knockdown promotes tumor progression *in vivo*.

Table 2
Comparison of expression of ER-related genes in PDAC microdissected lesions of the tumor epithelium *vs.* stroma.

Gene	log2FC	FDR
IGF1	−6.854	5.60E-19
MATN3	−6.476	2.74E-19
COL8A1	−6.428	3.30E-20
COL14A1	−6.423	1.15E-19
COL11A1	−6.267	2.21E-19
ISLR	−6.086	3.30E-20
TIMP3	−5.994	3.30E-20
COL15A1	−5.753	3.37E-20
HGF	−5.568	9.24E-19
FBN1	−5.555	3.30E-20
COL8A2	−5.506	6.80E-18
COL5A1	−5.482	3.30E-20
COL3A1	−5.420	3.30E-20
COL1A1	−5.309	3.30E-20
MXRA8	−5.296	3.33E-20
F13A1	−5.292	5.49E-18
COL6A3	−5.254	3.30E-20
COL10A1	−5.201	3.37E-20
SPON1	−5.187	3.28E-18
COL1A2	−5.128	3.30E-20
SPARC	−5.114	3.30E-20
PTGDS	−5.088	4.83E-15
IGFBP5	−5.075	6.34E-20
DOCK2	−5.039	9.94E-18
THBS4	−5.012	1.94E-14
COL5A2	−5.011	3.91E-20
COL24A1	−4.990	9.94E-18
CYR61	−4.984	3.93E-19
VWF	−4.903	4.93E-16
SPARCL1	−4.898	9.41E-20
FN1	−4.879	6.25E-20
CRISPLD2	−4.800	1.08E-19
COL4A1	−4.797	3.92E-20
DLC1	−4.784	6.68E-19
THBS1	−4.782	3.33E-20
MAN1C1	−4.772	5.08E-17
COL6A2	−4.727	7.74E-20
COL16A1	−4.710	3.92E-20
RARRES2	−4.702	4.07E-18
CRYAB	−4.682	2.63E-17
COL4A2	−4.662	4.49E-20
CHRDL1	−4.622	1.61E-13
TGFB3	−4.608	3.85E-17
IGFBP7	−4.606	3.30E-20
ADAMTSL1	−4.544	4.75E-17
SDC2	−4.544	3.30E-20
ADAMTS5	−4.529	7.98E-16
DPYSL3	−4.506	1.91E-19
WNT5A	−4.413	4.63E-19
LGALS1	−4.380	5.40E-19
RASGRF2	−4.349	1.59E-15
COL12A1	−4.327	3.37E-20
BCL2	−4.292	5.39E-16
SERPINE1	−4.280	2.36E-17
F2R	−4.222	1.83E-19
VEGFC	−4.147	5.60E-17
LRRK2	−4.121	9.28E-16
COL6A1	−4.114	4.41E-18
FSTL1	−4.045	3.30E-20
VCAN	−4.025	6.74E-20
A2M	−3.937	1.77E-19
FCGR2B	−3.832	3.08E-16
APOE	−3.827	1.06E-14
CDKN2B	−3.820	8.52E-14
IGFBP3	−3.805	2.51E-18
MAPK10	−3.780	1.30E-13
GPX7	−3.769	6.80E-13
SYT11	−3.766	5.45E-15
FKBP10	−3.666	3.86E-16
BAG2	−3.643	3.93E-14
GMFG	−3.579	1.24E-11
PDGFC	−3.572	3.32E-18
CCR5	−3.525	8.01E-12

(*continued on next page*)

Table 2 (*continued*)

Gene	log2FC	FDR
OSBPL6	−3.426	8.16E-13
PRSS23	−3.425	4.72E-19
KDELC1	−3.403	1.44E-12
FKBP7	−3.403	8.89E-18
LTBP1	−3.394	6.25E-20
FMO1	−3.384	2.72E-10
PDGFD	−3.379	2.65E-11
GPC3	−3.334	8.13E-11
P4HA3	−3.333	3.06E-13
HLA-DQA1	−3.323	6.67E-11
SERPING1	−3.315	2.50E-17
ARSB	−3.214	2.29E-15
MFGE8	−3.196	1.05E-15
ABCA1	−3.188	1.87E-19
STC2	−3.183	5.46E-11
CACNA1H	−3.141	1.71E-10
BIN2	−3.130	4.55E-13
CDH2	−3.088	1.56E-08
GPX8	−3.071	3.50E-18
COL4A5	−3.009	1.06E-10
SERPINH1	−2.909	2.30E-18
C3	−2.876	1.97E-09
CSF1	−2.843	4.91E-10
TRAM2	−2.831	5.90E-18
ARHGAP9	−2.830	9.73E-11
COL5A3	−2.776	5.93E-10
GAS6	−2.735	7.52E-12
ELOVL4	−2.719	7.71E-12
PKD2	−2.705	9.90E-18
LAMB1	−2.684	1.70E-19
TIMP2	−2.674	2.61E-18
SCG2	−2.605	2.78E-07
IGFBP4	−2.570	1.81E-17
F2RL3	−2.551	5.38E-11
CES1	−2.535	3.64E-09
FKBP14	−2.530	1.04E-14
SYTL4	−2.513	7.45E-13
BACE1	−2.486	2.46E-16
RYR2	−2.463	1.89E-06
ADAMTS7	−2.442	2.42E-07
S100A8	−2.435	2.17E-08
HLA-DQB1	−2.421	1.77E-06
FAM20C	−2.401	4.89E-10
FAM129A	−2.394	9.60E-11
RTN1	−2.379	5.27E-08
HLA-DRA	−2.280	2.12E-09
MAN1A1	−2.249	1.25E-14
TIMP1	−2.229	8.19E-16
ITPR1	−2.221	1.55E-11
TGFB1	−2.154	7.15E-10
VEGFB	−2.110	1.03E-09
FGR	−2.105	9.78E-07
COL4A4	−2.097	2.84E-05
GALNS	−2.088	1.75E-07
CRTAP	−2.085	1.50E-16
SYT1	−2.023	0.00020496
COL18A1	−1.959	1.10E-07
ARSG	−1.934	2.09E-07
CNIH3	−1.915	0.00018154
LAMB2	−1.910	5.07E-13
SLC37A2	−1.858	1.87E-05
TUSC3	−1.839	0.00041831
PYGL	−1.814	0.00030538
KDELC2	−1.807	8.09E-13
MMRN1	−1.804	9.13E-05
CD74	−1.748	1.43E-08
HLA-DRB5	−1.689	0.00023998
SEC23A	−1.678	8.70E-14
LAMC1	−1.636	5.01E-16
PADI2	−1.622	0.00133335
CALU	−1.604	3.93E-17
ADAMTSL4	−1.597	0.00186842
ATL1	−1.567	5.57E-06
VAT1	−1.545	3.28E-10
PROS1	−1.475	0.0001385
FTL	−1.436	1.46E-10

Table 2 (*continued*)

Gene	log2FC	FDR
FSTL3	−1.414	0.00603576
FERMT3	−1.403	0.00277423
SPP1	−1.383	0.00238724
GJB2	−1.371	9.08E-05
ARSK	−1.364	0.00095114
SLC35B4	−1.357	1.34E-06
CREB3L2	−1.353	7.84E-13
MAGED2	−1.342	2.96E-08
GM2A	−1.325	2.22E-07
CKAP4	−1.323	6.80E-10
HERPUD1	−1.308	2.27E-07
CNN2	−1.291	2.27E-08
TMX3	−1.271	1.48E-09
CFD	−1.267	0.00349052
PIK3R1	−1.265	1.00E-08
RPS6KA2	−1.252	8.62E-06
SEC24D	−1.229	2.55E-11
MAN2B1	−1.224	1.47E-05
ACTN1	−1.212	2.91E-12
TNC	−1.205	0.02913793
TGFB2	−1.201	0.01814096
ELOVL5	−1.185	2.29E-06
RGMB	−1.171	8.32E-05
COL7A1	−1.152	0.01652916
TP53	−1.127	0.04164063
F8	−1.112	0.00151011
FOXRED2	−1.101	0.01004867
NEU1	−1.100	0.05194287
TMTC3	−1.099	9.73E-08
RCN1	−1.093	7.10E-07
GSN	−1.076	2.72E-06
NUCB1	−1.076	0.00025704
CPPED1	−1.070	0.02217519
FKBP11	−1.068	0.004347
CEBPB	−1.036	0.00018513
TMCO1	1.003	7.45E-07
ELOVL1	1.012	0.0002326
TBL2	1.020	0.00063544
SRP9	1.040	1.99E-06
PIGG	1.040	0.00668933
SEC16B	1.054	0.01269919
APRT	1.055	0.00313812
BLOC1S3	1.075	0.00849932
LBR	1.075	3.29E-07
ARV1	1.082	0.00014765
ANXA2	1.093	2.49E-10
AIFM1	1.095	0.00162357
ACAA1	1.103	0.00269328
CSTB	1.108	1.07E-08
FUCA1	1.132	1.05E-05
HEBP2	1.133	6.95E-06
TMEM33	1.133	9.09E-10
SLC35B1	1.133	8.24E-05
OLA1	1.135	1.25E-09
TEX264	1.149	0.00428873
HSP90AA1	1.149	1.07E-13
CCDC115	1.151	0.00089106
H2AFZ	1.162	2.01E-07
UBQLN4	1.162	0.00100115
PSMA5	1.166	2.12E-05
PTGS2	1.169	0.00111025
EIF2AK1	1.170	1.19E-10
ARFGAP2	1.171	0.00551118
ATL2	1.176	1.20E-08
H2AFX	1.182	0.0041568
GSDMD	1.189	0.01408204
SORL1	1.203	2.14E-05
VWA1	1.208	0.00100718
TRAF2	1.216	0.00103768
SEC23B	1.220	3.70E-10
QSOX1	1.224	7.98E-08
UNC13D	1.232	0.00596797
DNAJB2	1.239	0.00124739
TMED4	1.251	5.21E-05
GCA	1.255	3.10E-06
ASPH	1.256	1.81E-09

(*continued on next page*)

Table 2 (*continued*)

Gene	log2FC	FDR
PSMD14	1.258	9.92E-07
DAB2IP	1.265	0.00018841
APLP2	1.270	3.93E-11
CAPN1	1.272	1.15E-07
VPS33B	1.281	0.00207547
PMM2	1.283	0.00015424
GAK	1.305	0.00011593
YOD1	1.311	2.66E-07
LMAN2L	1.315	0.00423172
TMEM170A	1.342	0.0001837
ZC3H12A	1.343	0.00412738
SCCPDH	1.349	1.71E-07
RNF103	1.354	3.33E-08
RPS6KA1	1.402	0.00090909
DNASE1L1	1.426	0.00042631
LYZ	1.442	5.17E-05
TECR	1.447	5.97E-08
GET4	1.459	0.00136111
BAK1	1.463	0.00016382
RNASET2	1.498	1.52E-06
CLN6	1.537	0.00016884
CTAGE5	1.550	1.39E-14
PIGU	1.554	2.67E-05
DSN1	1.596	0.00023102
GSTP1	1.601	1.41E-11
GOLM1	1.652	1.40E-12
PTGES2	1.658	1.86E-05
ZFYVE27	1.669	0.00020239
OSBPL3	1.674	3.19E-11
HPSE	1.677	4.20E-05
ARL6IP1	1.681	3.34E-13
PDCD6	1.692	2.96E-08
HSPBP1	1.695	1.78E-05
BCAP31	1.702	9.32E-11
PNPLA2	1.720	4.21E-07
CDA	1.726	0.00053269
HIST1H2BK	1.757	9.35E-10
BAG1	1.762	2.64E-09
IDH1	1.763	2.34E-13
NOL3	1.789	3.52E-06
SERPINB1	1.798	4.08E-10
DOLPP1	1.834	3.57E-06
CANT1	1.849	1.03E-08
PRKCD	2.004	4.21E-07
JUP	2.070	4.61E-14
SVIP	2.091	1.26E-09
REEP1	2.209	2.78E-05
OSBPL7	2.213	3.19E-07
PNP	2.287	7.67E-07
HIST1H2BD	2.342	3.90E-12
PYGB	2.410	5.88E-14
ELOVL6	2.418	1.46E-09
UBE2C	2.496	1.33E-07
SLC37A4	2.651	1.75E-09
SERPINA1	2.666	8.65E-11
RAB3D	2.714	9.55E-10
TMEM30B	2.726	1.09E-15
DHRS9	2.764	5.01E-05
SLC37A1	2.815	3.61E-12
CCNA2	2.877	1.77E-10
SERPINA3	2.909	7.68E-07
SYT17	2.973	6.37E-10
FRK	3.098	8.76E-16
F5	3.196	1.73E-11
PLAC8	3.199	7.44E-10
DHCR7	3.249	2.41E-12
TC2N	3.753	3.44E-19
TMEM97	3.772	9.64E-16
TGFA	3.791	3.54E-15
CP	3.926	8.89E-09
ELOVL7	4.252	2.68E-15
SGPP2	4.538	2.24E-16
SLPI	4.555	1.23E-16
LCN2	4.798	3.79E-14
MSLN	4.868	5.54E-15
SYT13	5.009	8.44E-14
OLFM4	5.669	1.89E-11
PROM1	5.817	1.02E-17
AGR2	5.986	2.14E-19

Overall, these findings demonstrate that FKBP7 expression in PSCs supports a tumor-inhibitory phenotype, consistent with FKBP7 *in vitro* effects on reducing PSC contractility and inflammatory secretion, thereby limiting tumor growth.

3.5. Restraining effect of PSCs expressing FKBP7 on tumor growth correlates with the formation of an encapsulating fibrous shell

Microscopic analysis of Sirius red-stained sections of MiaPaCa-2 and PSC co-xenografts under polarized light showed that tumors with FKBP7-expressing control PSCs (shCTR) exhibited both thick (yellow-orange) and thin (green) fibrillar collagens, which were significantly reduced when FKBP7 was knocked down in PSC^{KD} (Fig. 5A–B), despite driving larger tumor size (Fig. 4F–S5A).

Immunofluorescence revealed that FKBP7-expressing PSC tumors were encapsulated in a shell rich in fibronectin and types III and IV collagens (but low in type I collagen), effectively separating tumor cells (identifiable by high mutant p53 expression) from the surrounding acinar compartment. In contrast, FKBP7^{KD} PSC tumors showed no such separation, and the extracellular matrix (ECM) was remodeled with high type I collagen but low types III and IV collagens, alongside increased MMP-9 expression, enabling tumor cell invasion, which showed high expression of the epithelial-to-mesenchymal marker vimentin (Fig. 5C).

In vitro FKBP7 knockdown in FKBP7^{KD} PSCs increased type I collagen but reduced type IV collagen expression, while FKBP7 overexpression in FKBP7^{OE} PSCs had the opposite effect (Fig. 5D–E, S5B-D). Type I collagen fibers in FKBP7^{KD} PSCs were aligned, contrasting with the dispersed fibers seen in FKBP7-expressing shCTR PSCs (Fig. 5F). These findings indicate that *in vivo* control FKBP7-expressing PSCs promote the formation of types III/IV collagen and fibronectin-rich shell, which inhibits tumor growth and invasion, while FKBP7 loss within PSCs leads to the secretion of a type I collagen-dense, invasive ECM, fostering tumor progression.

3.6. Mechanism for FKBP7 effect in PSCs

Our study shows FKBP7 is more abundant in the membranous fraction compared to the cytosolic fraction in PSCs (Fig. 6A). As reported in another cell type [33], we confirmed FKBP7 complexes with BiP in PSCs, as BiP co-immunoprecipitated with an anti-FKBP7 antibody, though this interaction appears unstable as FKBP7 was not found in the BiP co-immunoprecipitate (Fig. 6B). Unlike in prostate cancer cells, where FKBP7 has been found in the translation initiation eIF4F complex as a direct interactor with eIF4G and has been shown to support cell resistance to taxanes *via* regulation of mRNA translation [34], FKBP7 did not co-immunoprecipitate with eIF4G in PSCs, thus suggesting a cell-specific role for FKBP7.

Despite BiP role in ER stress regulation, altering FKBP7 expression in FKBP7^{KD} PSCs, whether treated with UPR-activating drugs (thapsigargin), did not affect UPR markers (PERK and eIF2α phosphorylation, ATF4, IRE1α, BiP, spliced XBP1 expression) or cell survival, with similar outcomes in shCTR and FKBP7^{KD} cells (Figs. S6A–C).

We further explored FKBP7 domains to determine their role in the PSC phenotype (Figs. 3–5) by creating and overexpressing HA-tagged mutants lacking either the N-terminal (comprising the FKBP domain with the peptidyl-prolyl isomerase (PPI) activity) (FKBP7^{OE}ΔPPI) or the C-terminal domain (comprising two EF-hand motifs previously shown to be involved in binding to BiP) (FKBP7^{OE}Δcter) [33,50] (Fig. S6D). While FKBP7^{OE}ΔPPI binds BiP, FKBP7^{OE}Δcter does not (Fig. 6C–D).

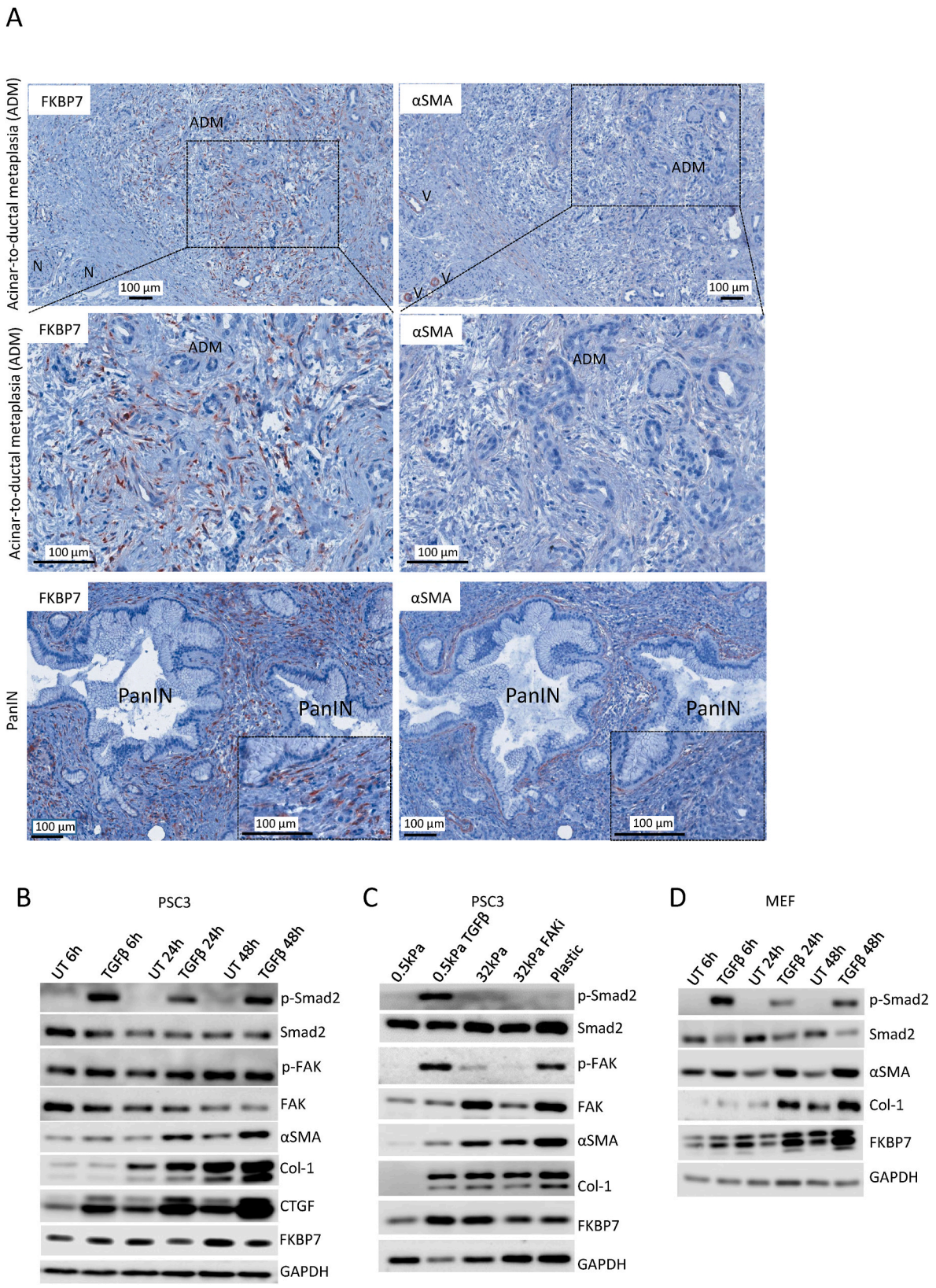

Fig. 2. FKBP7 expression is increased during PSC activation *in vivo* and *in vitro*.
A- Representative images of immunohistochemistry stainings of FKBP7 and αSMA on acinar-to-ductal metaplasia (ADM) and PanIN, observed at distance from PDAC lesions (N = 5 samples); N = nerve; V = vessel. **B-D**- Representative Western blots of human PSC3 treated or not (UT) with TGFβ (8 ng/mL) for 6h, 24h and 48h (B), or of human PSC3 plated for 7 days on soft (0.5 kPa) or stiff matrix (32 kPa), and treated or not (UT) with TGFβ (8 ng/mL) or with the FAK inhibitor (1 µM) for 24h (C), or of Mouse Embryonic Fibroblasts (MEF) treated or not (UT) with TGFβ (8 ng/mL) for 6h, 24h and 48h (D); blotting was performed with the phospho-smad2, smad2, phospho-FAK, FAK, αSMA, ColI, CTGF or FKBP7 antibody, GAPDH antibody serves as a loading control. N = 3 experiments.

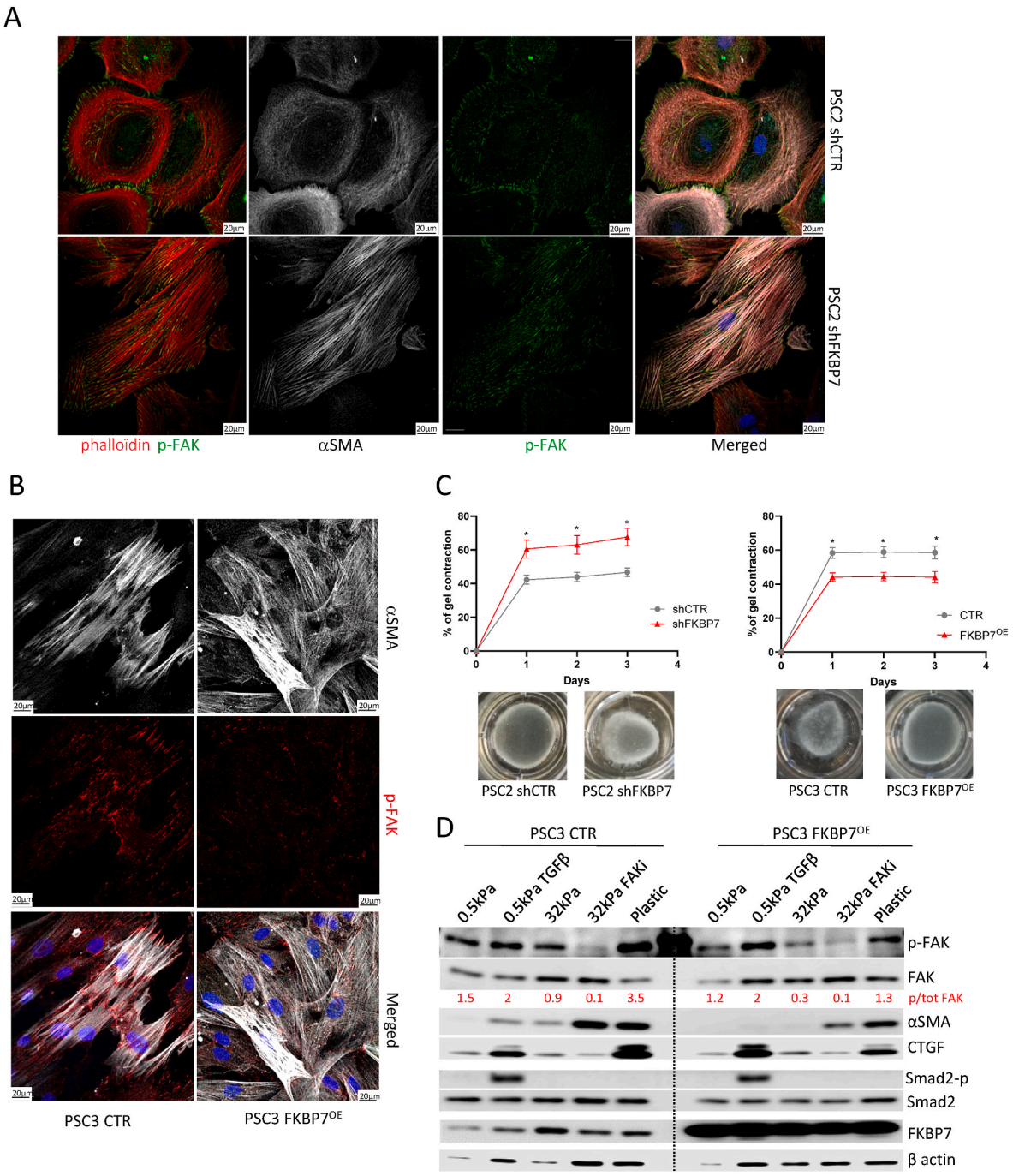

Fig. 3. FKBP7 expression impacts PSC morphology and restrains their activation.
A- Representative immunofluorescence staining (from left to right) of phalloidin/phospho-FAK, αSMA, phospho-FAK and the merge of all stainings, performed in shCTR (upper panel) and shFKBP7 (shRNA-1, lower panel) PSC2. N = 3 experiments. **B-** Representative immunofluorescence staining (from top to bottom) of αSMA, phospho-FAK and the merged of both stainings, performed in control PSC3 (CTR) in left panels, or PSC3 overexpressing FKBP7 (FKBP7^{OE}) in right panels. N = 3 experiments. **C-** Quantification of collagen I gel contraction induced for 3 days by shCTR vs. shFKBP7 (shRNA-1, left panels) PSC2, or by CTR vs. FKBP7^{OE} (right panels) PSC3. Values (mean, SEM) are from three independent experiments of triplicates, student t-test was used to generate p values, *p < 0.05. Representative images of collagen gels contracted by the respective PSCs. **D-** Representative Western blot of CTR PSC3 and FKBP7 -transduced PSC3 grown on 0.5 or 32 kPa matrix, or on plastic, and treated when indicated with TGFβ (8 ng/mL) or the FAK inhibitor (1 μM) for 24h; Are presented blots with phospho-FAK, FAK, and quantified ratio of p-FAK/total FAK, phospho-smad2, smad2, αSMA, CTGF and FKBP7 antibody, β actin antibody serves as a loading control. N = 3 experiments.

Overexpression of FKBP7^{OE}WT or FKBP7^{OE}ΔPPI reduced collagen gel contraction, FAK and MLC2 phosphorylation, whereas the FKBP7^{OE}Δcter increased both, mimicking FKBP7^{KD} knockdown effects (Fig. 6E–F, S6E-F). Consistently, overexpression of FKBP7^{OE}Δcter mutant, but not FKBP7^{OE}WT or FKBP7^{OE}ΔPPI, also enhanced type I collagen production (Fig. 6G–H). Instead, overexpression of FKBP7^{OE}WT in PSCs significantly increased type IV collagen expression (as already shown in Fig. 5E), as did transduction of the FKBP7^{OE}Δcter, but interestingly not the FKBP7^{OE}ΔPPI, resulting in similar type IV collagen production as in mock-transfected PSCs (Fig. 6I–J). Altogether these results demonstrate that FKBP7 enables type IV collagen production in PSCs in a manner dependent on its N-terminal domain

A

PSC2 – conditioned media

Down-regulated	% of shCTR	Up-regulated	% of shCTR
RANTES (CCL5)	42.77589464	IL-31	126.7257846
IGFBP-2 (IBP2)	43.27767255	IL-17A	129.0385171
CD14	43.77020152	IL-27 (C19orf10)	134.5645195
Thrombospondin-1	46.2380644	PF4	135.5914093
IL-5	53.01147325	IL-10	137.6217985
Complement C5	54.74303878	MCP-3 (CCL7)	142.2485162
Cripto-1 (TDGF1)	56.01885516	IL-22	142.3308513
BDNF	57.60138763	DPPIV	147.753166
IL-12 p70 (IL12B)	58.88764206	IL-24	151.2087706
BAFF (TNFS13B)	60.066537	MIF	155.56108
CD30 (TNFRSF8)	60.40218539	IL-8 (CXCL8)	155.9988803
Fas Ligand	61.33343006	Pentraxin-3	158.9926087
IGFBP-3 (IBP3)	63.54925113	PDGF-AA	160.5827165
GDF-15	64.57041565	PDGF-AB/BB	166.260657
CD40 ligand	65.88723568	Lipocalin-2 (LCN2)	172.6354283
IL-1alpha	66.5528146	LIF	188.8068965
Chitinase 3-like 1 (CHI3L1)	66.93576591	VCAM-1	194.1291661
Vitamin D BP (GC)	68.48216983	TFF3	204.3061181
Cystatin C	69.51821986	IL-6	249.1087779
IL-33 (IL1F11)	72.6926122	IL-23 (IL23A)	250.1341827
IL-1ra (IL1RN)	74.33277662		
MIG (CXCL9)	74.39300043		
IL-2	76.76876333		
MIP-3alpha (CCL20)	79.4195825		

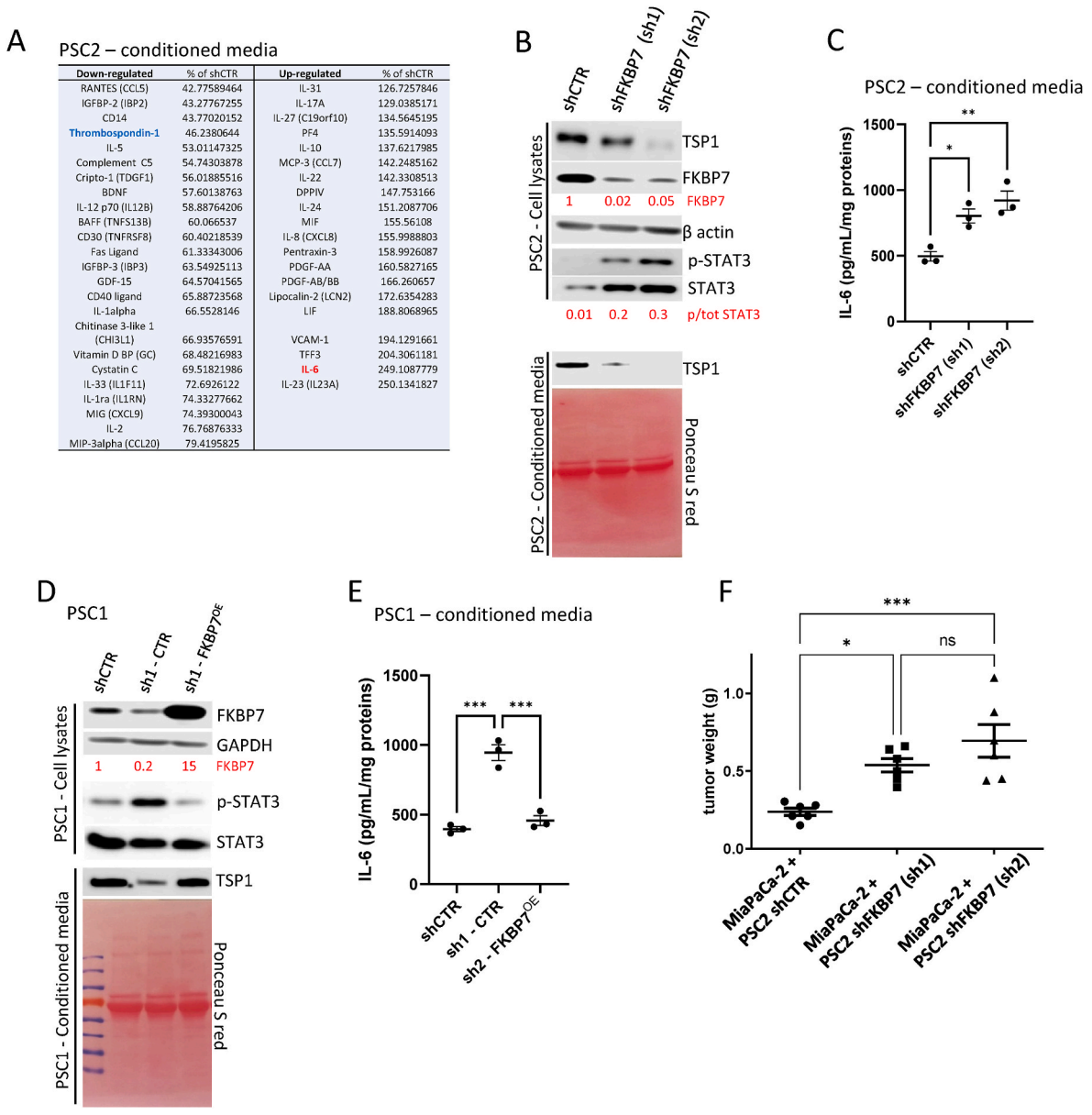

Fig. 4. FKBP7 inhibits FAK signaling pathway in PSCs, altered their secretome and is involved in PSC antitumoral properties *in vivo*
A- Table representing the list of proteins down-regulated or up-regulated in the conditioned media of shFKBP7 PSC2 compared to shCTR PSC2, as measured using a membrane antibody array assay; Values are mean fold changes of the two shFKBP7 compared to shCTR. **B-** Western blot performed on protein cell lysates (upper panels) or conditioned medium (lower panels) of shCTR PSC2 or shFKBP7 (shRNA-1 or shRNA-2) PSC2 with the TSP1 or FKBP7 or phospho-STAT3 and STAT3 antibody; β actin or Red ponceau serve as a loading control for cell lysates or conditioned media, respectively. **C-** ELISA for IL-6 on conditioned media (from 4B). ANOVA was used to generate p values, *$p < 0.05$ **$p < 0.01$. N = 3 experiments. **D-** Western blot performed on protein cell lysates (upper panels) or conditioned media (lower panels) of shCTR or shFKBP7 (shRNA-1) PSC1 rescued for FKBP7 ($FKBP7^{OE}$), with the FKBP7, phospho-STAT3, STAT3, or TSP1 antibody; GAPDH or Ponceau red serve as a loading control for cell lysates or conditioned medium, respectively. **E-** ELISA for IL-6 on conditioned media (from 4D). ANOVA was used to generate p values, ***$p < 0.001$. N = 3 experiments. **F-** MiaPaCa-2 cells were injected in the pancreas of nude mice, with shCTR PSC2 (n = 6 mice), or with shFKBP7 PSC2 (shRNA-1, n = 6 mice; shRNA-2, n = 6 mice). Tumor weight at the day of sacrifice was measured. Man-Whitney test was used to generate p values, *$p < 0.05$,** $p < 0.01$,***$p < 0.001$; ns, non significant.

(comprising the PPI activity), but not C-terminal domain. This is in contrast to the FKBP7-dependent inhibition of type I collagen production and PSC contractility, which requires the C-terminal domain of FKBP7 comprising the BiP-interaction domain.

4. Discussion

To identify ER-resident proteins that may support increased synthesis of membranous and secreted proteins during PSC activation into myofibroblasts, we examined FKBP7, an ER-resident peptidyl prolyl isomerase. Our analysis revealed that FKBP7 is overexpressed in the tumor stroma compared to the epithelium, and is specifically present in fibroblastic populations within PDAC tissue also expressing other reported CAF markers (ACTA2, FAP, POSTN, PDPN, PDGFRA) [8,51]. FKBP7 was detected at varying levels in PSCs and CAFs isolated from PDAC stromal tissue, though it was absent in tumor cells.

Given FKBP7 known interaction with the major ER chaperone BiP —where it negatively regulates BiP ATPase activity [33] —, and its role in protein synthesis regulation [34], we initially hypothesized that FKBP7 might regulate ER stress and protein synthesis in PSCs and CAFs.

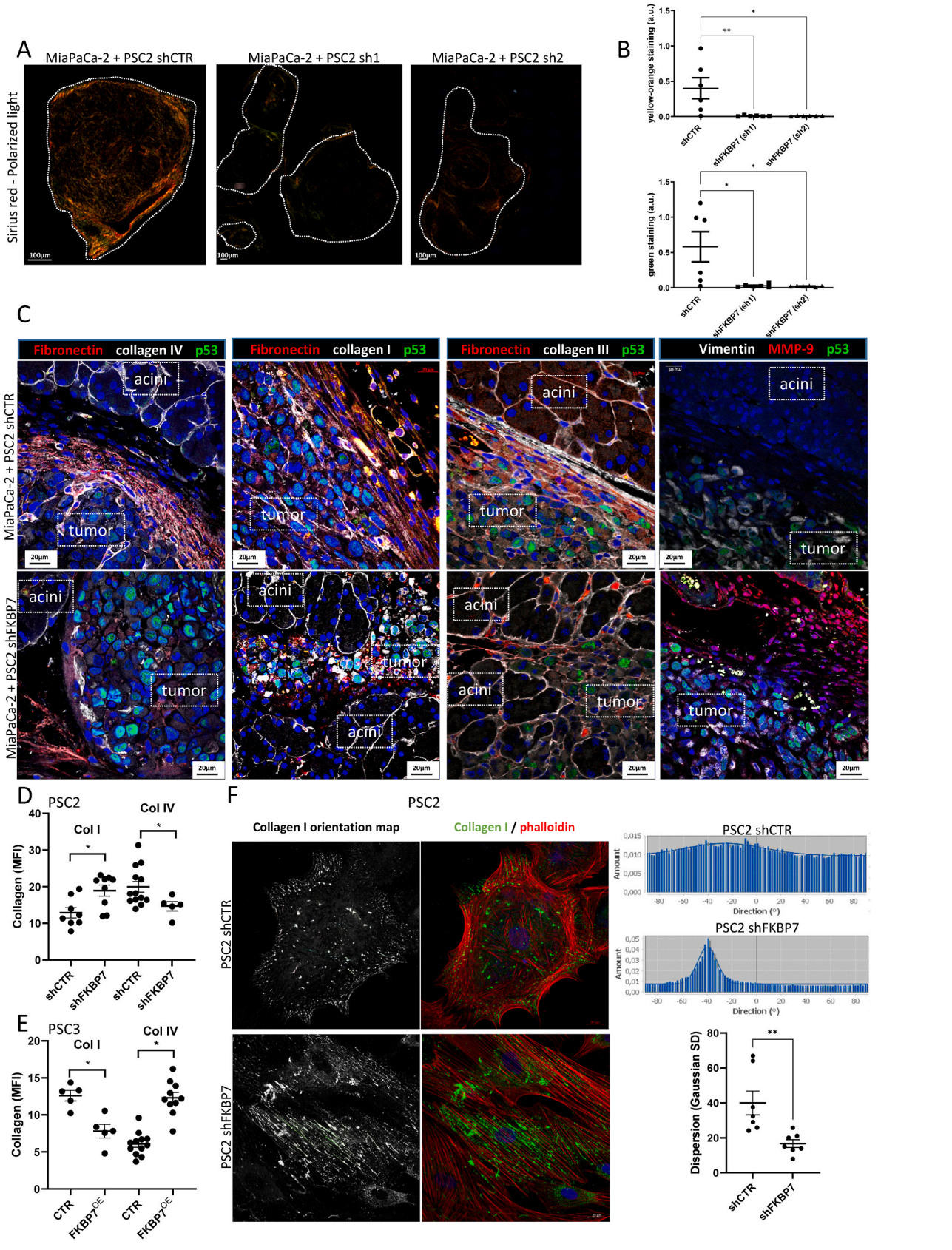

(caption on next page)

Fig. 5. Loss of FKBP7 expression in PSCs leads to a remodeling of the extracellular matrix both *in vivo* and *in vitro*.
A-B- Representative images of Sirius red coloration of tumors from mice grafted with MiaPaCa2 tumor cells + shCTR PSCs, or MiaPaCa2 tumor cells + shFKBP7 (shRNA-1 or shRNA-2) PSCs (from Fig. 4F), and analysis under polarized light microscopy with quantification of the yellow-orange and green collagen fibers in 6 tumors for each condition. ANOVA was used to generate p values, *$p < 0.05$. **C-** Representative immunohistofluorescence co-stainings (merged images) of (from left to right): fibronectin/type IV collagen/p53/DAPI, fibronectin/type I collagen/p53/DAPI, fibronectin/type III collagen/p53/DAPI, vimentin (human specific)/MMP9/p53/DAPI, performed on primary tumors (MiaPaCa2 + shCTR PSC2 (upper panel), and MiaPaCa2 + shFKB7 (shRNA-1) PSC2 (lower panel)). **D-E-** MFI quantification of type I or IV collagens performed in 5–12 ROI from immunofluorescence images obtained on shCTR or shFKBP7 (shRNA-1) PSC2 (Fig. S5C), and PSC3 transduced with FKBP7 ($FKBP7^{OE}$) or not (CTR) (Fig. S5D), using antibodies for type I or IV collagen, respectively. Student t-test was used to generate p values, *$p < 0.05$. N = 3 experiments. **F-** Representative analysis of type I collagen fiber alignment in shCTR or shFKBP7 (shRNA-1) PSC2. Are presented: orientation map image histograms indicating the amount of fibers in various directions (angle from −90° to 90°), the corresponding analyzed images (merging of type I collagen and phalloidin stainings), and the dispersion (standard deviation to Gaussian). Student t-test was used to generate p values, **$p < 0.01$. N = 7 ROI for each condition.

PSCs and CAFs produce and secrete more proteins and display greater resistance to ER stress-induced apoptosis than tumor cells. ER stress can induce fibroblast differentiation into myofibroblasts in fibrotic conditions, promoting both ER expansion and expression of αSMA, which supports ECM protein secretion and fibroblast contractility [52]. However, when we knocked down FKBP7 in PSCs, our results showed that FKBP7 does not influence ER stress, disproving our hypothesis.

Interestingly, FKBP7 expression was observed in patients in the stroma surrounding acinar pancreatitis lesions in chronic pancreatitis, as well as surrounding preneoplastic lesions such as acinar-to-ductal metaplasia (ADM) and PanIN, and around PDAC lesions, but not around vessels in pericytes or smooth muscle cells where αSMA is expressed. This expression pattern in the stroma, particularly around ADM where αSMA is absent, suggests that FKBP7 may act as an earlier marker of PSC activation than αSMA. Our experiments also demonstrated that FKBP7 expression in PSCs is increased by TGFβ and matrix stiffness, which are early triggers of PSC activation during pancreatic tumorigenesis, suggesting that FKBP7 may regulate these PSC activation programs. Since our PSCs and CAFs are isolated from tumors of patients who were eligible for surgical resection, they are presumably representative of early stage disease, and accordingly express high levels of FKBP7, albeit at different levels, which we have shown to be expressed in the stroma in correlation with improved survival of patients.

Our findings show that altering FKBP7 expression in PSCs produced opposite effects on cell phenotype. Low FKBP7-expressing PSCs (knockdown cells) exhibited larger contractile stress fibers, more adhesion sites, and increased FAK and Rho (p-MLC2) signaling. These cells were more contractile, secreted more pro-inflammatory cytokines (like LIF and IL6), and displayed higher STAT3 signaling—all features associated with a pro-tumorigenic, contractile phenotype with increased type I collagen production and deposition. When co-grafted with human pancreatic cancer cells in mice, these FKBP7 knockdown PSCs accelerated tumor progression and induced high levels of ECM remodeling (marked by MMP9 and type I collagen). In contrast, control PSCs in the tumors generated an encapsulating layer rich in types III and IV collagens and fibronectin, suggesting a more tumor-restraining environment. This aligns with our bioinformatics analysis showing that FKBP7 mRNA expression inversely correlates with "activated stroma" or "inflammatory CAF" signatures [48,49], and indicates that high FKBP7 levels in the stroma predict better survival outcomes for PDAC patients.

Our findings support a role for FKBP7 as a restraining factor in pancreatic tumorigenesis, similar to other tumor-suppressive fibroblasts such as those expressing meflin or lacking CD105 [53,54]. However, our findings contrast with the typical binary view of CAF subtypes, which are traditionally categorized as either inflammatory (iCAF) or myofibroblastic (myCAF), linked to JAK-STAT or TGFβ-SMAD pathway activation, respectively [55]. Notably, FKBP7 knockdown in PSCs led to both secretory inflammatory and contractile phenotypes, demonstrating PSC phenotypic plasticity. This shift between CAF phenotypes may involve epigenetic regulation, sustaining JAK1/STAT3 signaling and ECM remodeling, as reported in other cancers [19].

To explore how FKBP7 affects PSC contractility, we tested whether its N- and C-terminal domains, which contain one FKBP domain or two EF-hand domains and were previously reported to be involved in FKBP7 PPI activity and its interaction with BiP [50], respectively, play a role. Interestingly, BiP was described to modulate type I collagen lysyl hydroxylation, through the regulation of the formation of a complex comprising the lysyl hydroxylase 2 (LH2) and the two other chaperones HSP47 and FKBP10 [56]. Our results show that overexpression of a FKBP7 mutant lacking the BiP-binding domain ($FKBP7^{OE}\Delta$Cter) in PSCs increased contractility, FAK and Rho signaling, and type I collagen production, mirroring the effects of FKBP7 knockdown. Our data suggest a working model (Fig. S6G) whereby FKBP7 may limit type I collagen maturation through BiP interaction, presumably by titrating BiP away from the HSP47/FKBP10 complex, although we cannot exclude the involvement of other partners that bind the FKBP7 C-terminal domain; during tumor progression, decreased FKBP7 expression in cancer-activated PSCs may lead to increased type I collagen production by relieving FKBP7-dependent BiP blockade. Notably, FKBP7-expressing PSCs instead produce type IV collagen, which typically comprises the basal membrane in normal tissue and was abundant in the fibrous encapsulation seen in tumors with FKBP7-expressing PSCs. Such a "normalized" type IV collagen-rich ECM structure may be involved in the inhibition of tumor spread. The FKBP7 PPI activity may be required for type IV collagen production, as observed in PSCs overexpressing the $FKBP7^{OE}\Delta$PPI mutant, which showed decreased type IV collagen expression, albeit weak, consistent with the reported weak PPI activity of FKBP7 [57]. Altogether, we show that each domain of the FKBP7 protein is involved in specific regulation of collagens, negative *via* the C-terminal domain for type I collagen, or positive *via* the N-terminal domain for type IV collagen. Future research will focus on clarifying this mechanism, with the goal of developing therapeutic strategies that promote a balance favoring type IV collagen production over type I. Our work also suggests that FKBP7 and possibly other FKBP family proteins specifically regulate ER maturation of distinct collagen types, such as type I collagen in clear cell renal cell carcinoma for FKBP10 [56,58]. Interestingly, another hit found in our screen (Fig. 1D) is FKBP14, which is very similar to FKBP7 in that it also contains the two EF-hand domains in its C-terminus and an FKBP domain in its N-terminus. Thus, we cannot exclude its involvement as a regulator of PSC function, which has not yet been explored. Interestingly, mutations in the *FKBP14* gene cause kyphoscoliotic Ehlers-Danlos syndrome, which is characterized by a broad phenotypic outcome, probably explained by the fact that FKBP14 binds to types III, IV, and X collagens, and may be involved in their biosynthesis [59].

This study identifies a previously poorly described ER-residing chaperone, FKBP7, as an early marker of PSC activation, associated with improved prognosis in PDAC patients, and describes its role in restraining PSC-mediated pancreatic tumorigenesis by modulating the myofibroblastic contractile phenotype through BiP interaction. Understanding how ER chaperones like FKBP7 and BiP modulate myofibroblast activation and ECM composition by controlling the maturation of specific pro-tumor collagens could offer novel approaches to targeting the PDAC stroma.

CRediT authorship contribution statement

Christophe Quemerais: Writing – original draft, Visualization,

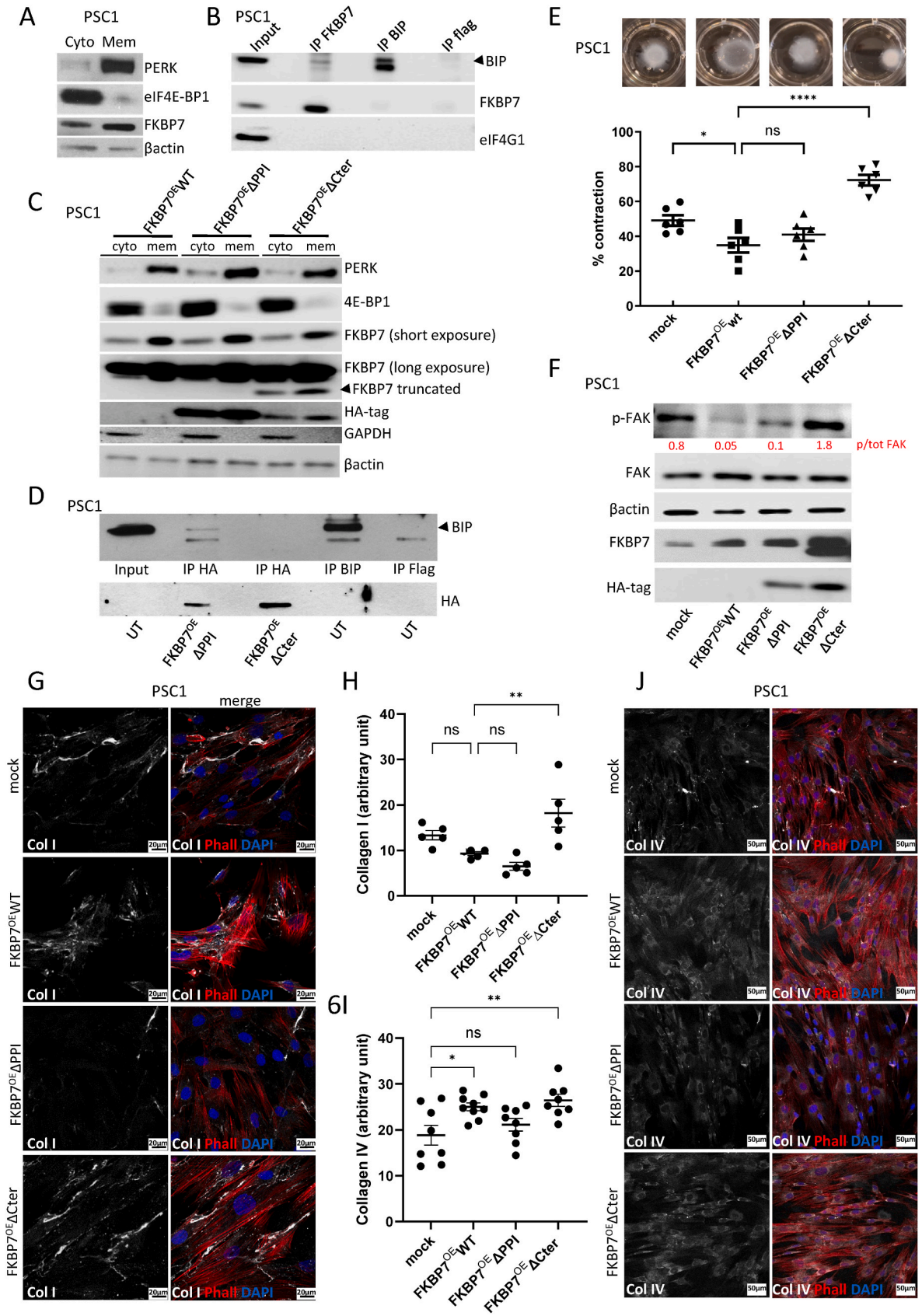

(caption on next page)

Fig. 6. Mechanism for FKBP7 effect in PSCs.
A- Representative Western blot after subcellular fractionation of PSC1 (cytosol and membranes) with PERK, eIF4E-BP1, and FKBP7 antibody. βactin antibody serves as loading control. N = 3 experiments. **B-** Representative Western blots after co-immunoprecipitation in PSC1 of FKBP7, or BIP (negative control). BIP, FKBP7 and eIF4G1 antibodies were used. Input represents 10 % of total immunoprecipitation. Irrelevant IP anti Flag serves as negative control. N = 3 experiments. **C-** Representative Western blots of PSC1 overexpressing FKBP7^{OE}WT, ΔPPI or ΔCter mutant, performed using protein extracts after subcellular fractionation (cyto: cytosol; mem: membranes), and showing expression of PERK, 4E-BP1, FKBP7 (blotted with an antibody specific to the Nter part of the protein), GAPDH and the HA-tagged FKBP7 mutants. 4E-BP1, GAPDH and βactin serve as loading controls for the cytosolic fraction, and PERK for the membrane fraction. N = 3 experiments. **D-** Representative Western blots after co-immunoprecipitation with the anti-HA antibody (IP HA) using protein extracts from PSC1 transduced or not (UT) with HA-tagged FKBP7 mutants (ΔPPI or ΔCter); Immunoprecipitation with the anti-BiP or irrelevant anti-Flag antibody was used as negative control. BiP and HA antibodies were used for blotting. Input represents 10 % of total immunoprecipitation. N = 3 experiments. **E-** Quantification of collagen type I gel contraction induced for 3 days by PSC1 transduced with empty vector (mock), or FKBP7^{OE}WT, or FKBP7^{OE}ΔPPI or FKBP7^{OE}ΔCter mutant. Values (mean, SEM) are from three independent experiments of triplicates. ANOVA was used to generate p values, *p < 0.05, ****p < 0.0001. Representative images of collagen gels contracted by the respective PSCs (upper panels). **F-** Representative Western blot of PSC1 transduced with empty vector (mock), or FKBP7^{OE}WT, or FKBP7^{OE}ΔPPI or FKBP7^{OE}ΔCter mutant; Are presented blots with phospho-FAK, FAK, and quantified ratio of p-FAK/total FAK, FKBP7 and HA antibody. β-actin antibody serves as a loading control. N = 3 experiments. **G-H-** Immunofluorescence on PSC1 transduced with empty vector (mock), or FKBP7^{OE}WT, or FKBP7^{OE}ΔPPI or FKBP7^{OE}ΔCter mutant, using antibody for type I collagen and phalloidin, and merged images (G), and associated MFI quantification of type I collagen in 5 ROI (H). ANOVA test was used to generate p values, **p < 0.01. N = 3 experiments. **I-J-** Immunofluorescence on PSC1 transduced with empty vector (mock), or FKBP7^{OE}WT, or FKBP7^{OE}ΔPPI or FKBP7^{OE}ΔCter mutant, using antibody to type IV collagen and phalloidin, and merged images (I), and associated MFI quantification in 5 ROI (J). ANOVA test was used to generate p values, *p < 0.05 **p < 0.01. N = 3 experiments.

Methodology, Investigation, Formal analysis, Conceptualization. **Christine Jean:** Writing – original draft, Methodology, Conceptualization. **Alexia Brunel:** Methodology. **Emilie Decaup:** Methodology, Investigation. **Guillaume Labrousse:** Methodology. **Hippolyte Audureau:** Investigation. **Jérôme Raffenne:** Investigation. **Ismahane Belhabib:** Investigation. **Jérôme Cros:** Visualization, Resources, Investigation. **Aurélie Perraud:** Investigation. **Nelson Dusetti:** Resources. **Remy Nicolle:** Resources, Investigation, Data curation. **Muriel Mathonnet:** Resources. **Stéphane Pyronnet:** Supervision, Project administration, Funding acquisition, Conceptualization. **Yvan Martineau:** Writing – original draft, Methodology, Investigation, Conceptualization. **Marjorie Fanjul:** Writing – original draft, Supervision, Resources, Methodology, Investigation, Formal analysis, Data curation, Conceptualization. **Corinne Bousquet:** Visualization, Validation, Supervision, Project administration, Methodology, Investigation, Funding acquisition, Formal analysis, Conceptualization.

Declaration of generative AI and AI-assisted technologies in the writing process

Statement: During the preparation of this work the author(s) used ChatGPT in order to improve the readability and language. After using this tool/service, the author(s) reviewed and edited the content as needed and take(s) full responsibility for the content of the published article.

Funding

This work was supported by LNCC (Equipe Labellisée LIGUE Contre le Cancer EL2021) and the French National Institute of Cancer (INCa PAIR18-080). C.Q., H.A. and I.B. were recipients of a fellowship from the Ligue Nationale Contre le Cancer (LNCC). A.B. was recipient of a fellowship from the Fondation pour la Recherche Médicale.

Declaration of competing interest

The authors declare that they have no known competing financial interests or personal relationships that could have appeared to influence the work reported in this paper.

I, Corinne Bousquet and Corresponding Author for this manuscript, certify in the name of my co-Authors that they have no known competing financial interests or personal relationships that could have appeared to influence the work reported in this paper.

Acknowledgements

Authors acknowledge Christian Touriol (CRCT, France) for helpful discussion on ER stress; Authors acknowledge the CRCT core technology platform including Loïc Van Den Berghe for viral particle production and Laetitia Ligat for Imaging, the CREFRE animal facility, as well as Fabien Gava (Team NoLymIT, CRCT) for his help developing HCS analyses, JR Analytics for the bioinformatic analyses, and the CMEAB platform (Centre de Microscopie Electronique Appliquée à la Biologie, Toulouse Paul Sabatier University, France). Selected artwork shown in the graphical abstract were used from or adapted from pictures provided by Servier Medical Art (Servier; https://smart.servier.com/).

Appendix A. Supplementary data

Supplementary data to this article can be found online at https://doi.org/10.1016/j.canlet.2025.217538.

References

[1] J. Kleeff, et al., Pancreatic cancer, Nat. Rev. Dis. Primers 2 (2016) 16022.
[2] J.P. Neoptolemos, et al., Therapeutic developments in pancreatic cancer: current and future perspectives, Nat. Rev. Gastroenterol. Hepatol. 15 (6) (2018) 333–348.
[3] C. Neuzillet, et al., State of the art and future directions of pancreatic ductal adenocarcinoma therapy, Pharmacol. Ther. 155 (2015) 80–104.
[4] D. Salas-Benito, et al., Paradigms on immunotherapy Combinations with chemotherapy, Cancer Discov. 11 (6) (2021) 1353–1367.
[5] M.H. Sherman, G.L. Beatty, Tumor microenvironment in pancreatic cancer pathogenesis and therapeutic resistance, Annu. Rev. Pathol. 18 (2023) 123–148.
[6] M. Erkan, et al., The impact of the activated stroma on pancreatic ductal adenocarcinoma biology and therapy resistance, Curr. Mol. Med. 12 (3) (2012) 288–303.
[7] E. Hessmann, et al., Microenvironmental determinants of pancreatic cancer, Physiol. Rev. 100 (4) (2020) 1707–1751.
[8] G. Caligiuri, D.A. Tuveson, Activated fibroblasts in cancer: perspectives and challenges, Cancer Cell 41 (3) (2023) 434–449.
[9] H. Laklai, et al., Genotype tunes pancreatic ductal adenocarcinoma tissue tension to induce matricellular fibrosis and tumor progression, Nat Med 22 (5) (2016) 497–505.
[10] V.S. LeBleu, R. Kalluri, A peek into cancer-associated fibroblasts: origins, functions and translational impact, Dis Model Mech 11 (4) (2018).
[11] B. Hinz, D. Lagares, Evasion of apoptosis by myofibroblasts: a hallmark of fibrotic diseases, Nat. Rev. Rheumatol. 16 (1) (2020) 11–31.
[12] C.J. Tape, et al., Oncogenic KRAS regulates tumor cell signaling via stromal reciprocation, Cell 165 (7) (2016) 1818.
[13] M.A. Collins, et al., Oncogenic Kras is required for both the initiation and maintenance of pancreatic cancer in mice, J. Clin. Investig. 122 (2) (2012) 639–653.
[14] D. Kpeglo, et al., Modeling the mechanical stiffness of pancreatic ductal adenocarcinoma, Matrix Biol. 14 (2022) 100109.
[15] P.J. Wipff, et al., Myofibroblast contraction activates latent TGF-beta1 from the extracellular matrix, J. Cell Biol. 179 (6) (2007) 1311–1323.
[16] B. Piersma, M.K. Hayward, V.M. Weaver, Fibrosis and cancer: a strained relationship, Biochim. Biophys. Acta Rev. Canc 1873 (2) (2020) 188356.
[17] C. Gaggioli, et al., Fibroblast-led collective invasion of carcinoma cells with differing roles for RhoGTPases in leading and following cells, Nat. Cell Biol. 9 (12) (2007) 1392–1400.

[18] S. Zaghdoudi, et al., FAK activity in cancer-associated fibroblasts is a prognostic marker and a druggable key metastatic player in pancreatic cancer, EMBO Mol. Med. 12 (11) (2020) e12010.
[19] J. Albrengues, et al., Epigenetic switch drives the conversion of fibroblasts into proinvasive cancer-associated fibroblasts, Nat. Commun. 6 (2015) 10204.
[20] C. Duluc, et al., Pharmacological targeting of the protein synthesis mTOR/4E-BP1 pathway in cancer-associated fibroblasts abrogates pancreatic tumour chemoresistance, EMBO Mol. Med. 7 (6) (2015) 735–753.
[21] C. Vennin, et al., Reshaping the tumor stroma for treatment of pancreatic cancer, Gastroenterology 154 (4) (2018) 820–838.
[22] B.C. Ozdemir, et al., Depletion of carcinoma-associated fibroblasts and fibrosis induces immunosuppression and accelerates pancreas cancer with reduced survival, Cancer Cell 25 (6) (2014) 719–734.
[23] A.D. Rhim, et al., Stromal elements act to restrain, rather than support, pancreatic ductal adenocarcinoma, Cancer Cell 25 (6) (2014) 735–747.
[24] D.V. Catenacci, et al., Randomized phase ib/II study of gemcitabine plus placebo or vismodegib, a hedgehog pathway inhibitor, in patients with metastatic pancreatic cancer, J. Clin. Oncol. 33 (36) (2015) 4284–4292.
[25] E. Van Cutsem, et al., Randomized phase III trial of pegvorhyaluronidase alfa with nab-paclitaxel plus gemcitabine for patients with hyaluronan-high metastatic pancreatic adenocarcinoma, J. Clin. Oncol. (2020) Jco2000590.
[26] N. Hakim, et al., Why HALO 301 failed and implications for treatment of pancreatic cancer, Pancreas 3 (1) (2019) e1–e4.
[27] A. Hauge, E.K. Rofstad, Antifibrotic therapy to normalize the tumor microenvironment, J. Transl. Med. 18 (1) (2020) 207.
[28] K.Y. Elahi-Gedwillo, et al., Antifibrotic therapy disrupts stromal barriers and modulates the immune landscape in pancreatic ductal adenocarcinoma, Cancer Res. 79 (2) (2019) 372–386.
[29] J. Gore, M. Korc, Pancreatic cancer stroma: friend or foe? Cancer Cell 25 (6) (2014) 711–712.
[30] W.J. Ho, E.M. Jaffee, L. Zheng, The tumour microenvironment in pancreatic cancer - clinical challenges and opportunities, Nat. Rev. Clin. Oncol. 17 (9) (2020) 527–540.
[31] Z. Sun, J.L. Brodsky, Protein quality control in the secretory pathway, J. Cell Biol. 218 (10) (2019) 3171–3187.
[32] G.E. Karagoz, D. Acosta-Alvear, P. Walter, The unfolded protein response: detecting and responding to fluctuations in the protein-folding capacity of the endoplasmic reticulum, Cold Spring Harb Perspect Biol 11 (9) (2019).
[33] M. Feng, et al., Mouse FKBP23 mediates conformer-specific functions of BiP by catalyzing Pro117 cis/trans isomerization, Biochem. Biophys. Res. Commun. 408 (4) (2011) 537–540.
[34] M.F. Garrido, et al., Regulation of eIF4F translation initiation complex by the peptidyl prolyl isomerase FKBP7 in taxane-resistant prostate cancer, Clin. Cancer Res. 25 (2) (2019) 710–723.
[35] M.G. Bachem, et al., Identification, culture, and characterization of pancreatic stellate cells in rats and humans, Gastroenterology 115 (2) (1998) 421–432.
[36] M.V. Apte, et al., Periacinar stellate shaped cells in rat pancreas: identification, isolation, and culture, Gut 43 (1) (1998) 128–133.
[37] E.K. Schmidt, et al., SUnSET, a nonradioactive method to monitor protein synthesis, Nat. Methods 6 (4) (2009) 275–277.
[38] S. Weigle, et al., Primary cell-based phenotypic assays to pharmacologically and genetically study fibrotic diseases in vitro, J Biol Methods 6 (2) (2019) e115.
[39] S.R. Hingorani, et al., Trp53R172H and KrasG12D cooperate to promote chromosomal instability and widely metastatic pancreatic ductal adenocarcinoma in mice, Cancer Cell 7 (5) (2005) 469–483.
[40] R. Samain, et al., Pharmacologic normalization of pancreatic cancer-associated fibroblast secretome impairs prometastatic cross-talk with macrophages, Cell. Mol. Gastroenterol. Hepatol. 11 (5) (2021) 1405–1436.
[41] R. Nicolle, et al., Pancreatic adenocarcinoma therapeutic targets revealed by tumor-stroma cross-talk analyses in patient-derived xenografts, Cell Rep. 21 (9) (2017) 2458–2470.
[42] C. Maurer, et al., Experimental microdissection enables functional harmonisation of pancreatic cancer subtypes, Gut 68 (6) (2019) 1034–1043.
[43] J. Peng, et al., Single-cell RNA-seq highlights intra-tumoral heterogeneity and malignant progression in pancreatic ductal adenocarcinoma, Cell Res. 29 (9) (2019) 725–738.
[44] Z. Zhang, et al., SCINA: a semi-supervised subtyping algorithm of single cells and bulk samples, Genes 10 (7) (2019).
[45] E. Becht, et al., Estimating the population abundance of tissue-infiltrating immune and stromal cell populations using gene expression, Genome Biol. 17 (1) (2016) 218.
[46] S. Hänzelmann, R. Castelo, J. Guinney, GSVA: gene set variation analysis for microarray and RNA-seq data, BMC Bioinf. 14 (2013) 7.
[47] C. Neuzillet, et al., Inter- and intra-tumoural heterogeneity in cancer-associated fibroblasts of human pancreatic ductal adenocarcinoma, J. Pathol. 248 (1) (2019) 51–65.
[48] F. Puleo, et al., Stratification of pancreatic ductal adenocarcinomas based on tumor and microenvironment features, Gastroenterology 155 (6) (2018) 1999–2013.
[49] C.X. Dominguez, et al., Single-cell RNA sequencing reveals stromal evolution into LRRC15(+) myofibroblasts as a determinant of patient response to cancer immunotherapy, Cancer Discov. 10 (2) (2020) 232–253.
[50] X. Zhang, et al., The mouse FKBP23 binds to BiP in ER and the binding of C-terminal domain is interrelated with Ca2+ concentration, FEBS Lett. 559 (1–3) (2004) 57–60.
[51] C. Neuzillet, et al., Periostin- and podoplanin- positive cancer-associated fibroblast subtypes cooperate to shape the inflamed tumor microenvironment in aggressive pancreatic adenocarcinoma, J. Pathol. 258 (4) (2022) 408–425.
[52] F. Heindryckx, et al., Endoplasmic reticulum stress enhances fibrosis through IRE1α-mediated degradation of miR-150 and XBP-1 splicing, EMBO Mol. Med. 8 (7) (2016) 729–744.
[53] C. Hutton, et al., Single-cell analysis defines a pancreatic fibroblast lineage that supports anti-tumor immunity, Cancer Cell 39 (9) (2021) 1227–1244.e20.
[54] Y. Mizutani, et al., Meflin-positive cancer-associated fibroblasts inhibit pancreatic carcinogenesis, Cancer Res. 79 (20) (2019) 5367–5381.
[55] G. Biffi, et al., IL1-Induced JAK/STAT signaling is antagonized by TGFbeta to shape CAF heterogeneity in pancreatic ductal adenocarcinoma, Cancer Discov. 9 (2) (2019) 282–301.
[56] I. Duran, et al., A chaperone complex formed by HSP47, FKBP65, and BiP modulates telopeptide lysyl hydroxylation of type I procollagen, J. Bone Miner. Res. 32 (6) (2017) 1309–1319.
[57] Y. Ishikawa, K. Mizuno, H.P. Bächinger, Ziploc-ing the structure 2.0: endoplasmic reticulum-resident peptidyl prolyl isomerases show different activities toward hydroxyproline, J. Biol. Chem. 292 (22) (2017) 9273–9282.
[58] Y. Zhang, et al., FK506 binding protein 10: a key actor of collagen crosslinking in clear cell renal cell carcinoma, Aging (Albany NY) 13 (15) (2021) 19475–19485.
[59] Y. Ishikawa, et al., Local net charge state of collagen triple helix is a determinant of FKBP22 binding to collagen III, Int. J. Mol. Sci. 24 (20) (2023).